bioRxiv preprint doi: https://doi.org/10.1101/441162; this version posted October 11, 2018. The copyright holder for this preprint (which was not certified by peer review) is the author/funder, who has granted bioRxiv a license to display the preprint in perpetuity. It is made available under a CC-BY 4.0 International license.

Calotropis gigantea extract induces apoptosis through extrinsic/intrinsic pathways and upregulation of reactive oxygen species in non-small-cell lung cancer cells

Short title: Effects of CG Extract in non-small-cell lung cancer cells

Jiyon Lee[1], Huiju Jang[1], Yesol Bak[1], Jong-Woon Shin[1], Hang Jin[2], Yong-In Kim[3], Hyung Won Ryu[4], Sei Ryang Oh[4], Do-Young Yoon[1]*

[1] Department of Bioscience and Biotechnology, Konkuk University, Seoul 05209, Korea, [2] Institute of Medicinal Plants, Yunnan Academy of Agricultural Sciences (YAAS), 2238 Beijing Road, Kunming, Yunnan Province 650205, China, [3] International Biological Material Research Center, Korea Research Institute of Bioscience and Biotechnology, Daejeon 34141, Korea, [4] Natural Medicine Research Center, Korea Research Institute of Bioscience & Biotechnology (KRIBB), Cheongju 28116, Korea

***Corresponding author:**

E-mail: ydy4218@konkuk.ac.kr (D.Y. Yoon)

bioRxiv preprint doi: https://doi.org/10.1101/441162; this version posted October 11, 2018. The copyright holder for this preprint (which was not certified by peer review) is the author/funder, who has granted bioRxiv a license to display the preprint in perpetuity. It is made available under a CC-BY 4.0 International license.

Abstract

Background: *Calotropis gigantea* (CG) plant grows in Asia and tropical Africa. However, the precise mechanisms of its anticancer effects have not yet been examined in human non-small cell lung cancer (NSCLC) cells, A549 and NCI-H1299 cells.

Purpose: This study was focused on the anti-cancer effects of CG extract on non-small cell lung cancer (NSCLC) cells.

Methods: The cytotoxic effects of CG extract on NSCLC, A549 and NCI-H1299 cells, were detected by MTS assay, microscope and DAPI staining. Apoptosis was determined by annexin V-FITC/PI staining, cell cycle analysis, western blotting, quantitative polymerase chain reaction, and JC-1 staining.

Results: First, CG showed significant dose-dependent cytotoxicity in NSCLC, A549, and NCI-H1299 cells. In addition to induction of caspase-8 processing, CG induced apoptosis by upregulating mRNA expression levels of extrinsic pathway molecules such as Fas, Fas ligand (FasL), Fas-associated protein with death domain (FADD) and death receptor 5 (DR5). Also, mitochondrial membrane potential (MMP) was collapsed, and intrinsic pathway molecules such as poly (ADP-ribose) polymerase (PARP), caspase-3, and caspase-9 were processed by CG. Moreover, reactive oxygen species (ROS) were generated in a CG dose-dependent manner, and inhibition of ROS by NAC, ROS scavenger, recovered A549 and NCI-H1299 cell viability.

Conclusion: These results indicate that CG causes apoptosis by activating the extrinsic and intrinsic pathways and generating ROS in NSCLC cells. These results suggest that CG can be used as a lung cancer therapeutic agent.

Keyword: Apoptosis, non-small cell lung cancer, *Calotropis gigantea*, anti-cancer, intrinsic and extrinsic pathways, ROS

Abbreviations used: CG, *Calotropis gigantea*; NSCLC, non-small cell lung cancer; FasL, Fas Ligand; FADD, Fas-associated protein with death domain; DR5, death receptor 5; PARP, poly (ADP-ribose) polymerase; ROS, reactive oxygen species

bioRxiv preprint doi: https://doi.org/10.1101/441162; this version posted October 11, 2018. The copyright holder for this preprint (which was not certified by peer review) is the author/funder, who has granted bioRxiv a license to display the preprint in perpetuity. It is made available under a CC-BY 4.0 International license.

Introduction

Lung cancer, also known as lung carcinoma, is one of the most common diseases in the world [1]. However, owing to very few therapies being available, diverse studies on lung cancer are needed. Lung cancer is classified into non-small cell lung cancers (NSCLCs) and small cell lung cancers (SCLCs) [2, 3]. SCLC is a neuroendocrine tumor type, and the size of cells in these cancers is smaller than those in NSCLC. In contrast, NSCLC includes squamous cell carcinomas, large cell carcinomas, and adenocarcinomas. Among these NSCLCs, A549 lung cancer cells (wild-type p53) [4] and p53 null NCI-H1299 lung cancer cells are human non-small cell lung carcinoma cell lines.

Lung cancer is caused by uncontrolled cell growth in lung tissues because of defects in cancer suppressor genes [5], which results in the failure of apoptotic signaling and thus cell proliferation. In other words, inducing programmed cell death significantly reduces cancer cell numbers [6]. Apoptosis is a process of programmed cell death that controls cell division. If cells are old, our body causes them to commit suicide by activating an intracellular death process. Cells die by two apoptotic pathways: the intrinsic pathway and extrinsic pathway. First, the intrinsic pathway of apoptosis starts when the mitochondria outer membrane becomes permeable in response to intracellular stressors such as DNA damage, growth factor impairment, or oncogene activation. Cytochrome c and pro-apoptosis proteins are released from permeable mitochondria in a Bax/Bak-dependent manner [7]. These releases are regulated by Bcl-2 family members such as Bcl-2 and Bcl-xL and BH-3 family members such as Bid. Bax and Bak are activated by members of the BH-3 family [8] and inhibited by members of the Bcl-2 family. Through the association of these proteins, cytochrome c forms a complex, the apoptosome [9], which is composed of cytochrome c and caspase-9. Caspase-9 is activated by the apoptosome, and cleaved caspase-9 promotes activation of caspase-3 and inactivation of poly (ADP-ribose) polymerase (PARP), whose function is DNA damage repair [10]. Through this mechanism, this pathway induces apoptosis of cells. Second, two direct mechanisms of extrinsic pathway initiation have been described. One is the tumor necrosis factor (TNF)-induced model, and the other is the Fas-FasL-mediated model. Ligand binding with the receptor recruits adaptor proteins such as FADD and TRADD [11] and initiators such as pro-caspase-8 and pro-caspase-10. These complexes activate caspase-8 and caspase-10. Cleaved caspase-8 induces apoptosis by cleaving caspase-3. In addition, the extrinsic and intrinsic pathways are associated with caspase 8, which cleaves Bid into truncated Bid (tBid), the activated form of the protein. tBid induces the Bax/Bak-dependent release of cytochrome c. Finally,

bioRxiv preprint doi: https://doi.org/10.1101/441162; this version posted October 11, 2018. The copyright holder for this preprint (which was not certified by peer review) is the author/funder, who has granted bioRxiv a license to display the preprint in perpetuity. It is made available under a CC-BY 4.0 International license.

cleaved caspase-3 and inactivated PARP are triggered through both apoptotic pathways to dismantle the cells [12].

Programmed cell death can be initiated by various types of stress-induced damage. Reaction oxygen species (ROS) production [13] is a critical stressor that causes cell death, especially through the induction of apoptosis. Several reports have shown that ROS plays in important role in the apoptosis of cancer cells. The production of ROS such as $^{\bullet}OH$, O_2^-, and H_2O_2, caused by various external stimuli, is related to the inhibition of cell proliferation [14]. Low doses of H_2O_2 produce $^{\bullet}OH$ radicals, and an alternative oxidant/antioxidant pathway induces apoptosis. Furthermore, Bcl-2 controls not only apoptotic death but also the antioxidant pathway [15]. Cytochrome c release is suppressed by Bcl-2, and superoxide production is prevented when Bcl-2 is overexpressed [16]. In the cascade, a higher oxidant concentration decreases cell proliferation and finally induces apoptosis.

Calotropis gigantea (CG) is a tall and waxy flower that is mainly distributed in Cambodia, Indonesia, Malaysia, the Philippines, Thailand, Sri Lanka, India, China, Pakistan, Nepal, and tropical Africa. A hypoglycemic effect of the extract of flowers and leaves of CG [17] has been shown, with serum glucose levels that decreased with CG extract treatment. However, the presence of an anti-cancer effect of CG extract on lung cancer cells has not been assessed. Here, we report the presence of apoptosis signaling when lung cancer cells were treated with CG extract. Our results indicate a potential anti-cancer effect of CG extract on lung cancer cells.

bioRxiv preprint doi: https://doi.org/10.1101/441162; this version posted October 11, 2018. The copyright holder for this preprint (which was not certified by peer review) is the author/funder, who has granted bioRxiv a license to display the preprint in perpetuity. It is made available under a CC-BY 4.0 International license.

Materials and Methods

Reagents and antibodies

A stock solution of CG (30 mg/mL) in dimethyl sulfoxide (DMSO) was stored in the dark at −20°C and diluted in Rowell Park Memorial Institute (RPMI)-1640 medium immediately before use. CellTiter 96® AQueous One Solution Cell Proliferation Assay Reagent [MTS, 3-(4,5-dimethylthiazol-2-yl)-5-(3-carboxymethoxyphenyl)-2-(4-sulfophenyl)-2H-tetrazolium] was purchased from Promega (Madison, WI, USA), and propidium iodide (PI) was from Sigma-Aldrich (St. Louis, MO, USA). Antibodies specific to PARP, caspase-3, caspase-8, caspase-9, Bcl-2, Bcl-xL, Bax, Bid, and cytochrome c were from Cell Signaling Technology (Beverly, MA, USA). The anti-rabbit IgG horseradish peroxidase (HRP)-conjugated secondary antibody and anti-mouse IgG HRP-conjugated secondary antibody were from Millipore (Billerica, MA, USA). Antibodies specific to p21, p27, cyclin D1, cyclin E, cyclin A, and glyceraldehyde 3-phosphate dehydrogenase (GAPDH) were purchased from Santa Cruz Biotechnology (Santa Cruz, CA, USA). JC-1 (5,50,6,60-tetrachloro-1,10,3,30-tetraethyl benzimidazoly carbocyanine chloride) was obtained from Enzo (New York, USA), and FITC-annexin V apoptosis detection kit I was purchased from BD Biosciences (San Diego, CA, USA). DCF-DA was procured from Abcam (Cambridge, UK).

Plant material and preparation

Ethanol extract of whole plant of *C. gigantea* (L.) W.T. Aiton (Asclepiadaceae) was supplied by Foreign Plant Extract Bank (no. FBM085-042; Daejeon, Korea). The plant was collected in Yunnan Province of China in 2008 and authenticated by Jin Hang, The Chief of Medicinal Plants Research Institute, Yunnan Academy of Agricultural Sciences (YAAS) (Yunnan, China). A voucher specimen (YASS3533-2) is kept at the herbarium of YAAS. In preparation steps, the air-dried whole plant of *C. gigantea* sample (100.0 g) was mixed in 95% ethanol (800 mL × 2), and the mixture was shaken at room temperature for 2 h. The extracts were combined and concentrated in vacuo at 40 °C to produce a dried extract, which was used for phytochemical analysis and biological activities.

bioRxiv preprint doi: https://doi.org/10.1101/441162; this version posted October 11, 2018. The copyright holder for this preprint (which was not certified by peer review) is the author/funder, who has granted bioRxiv a license to display the preprint in perpetuity. It is made available under a CC-BY 4.0 International license.

116 **UPLC-QTof-MS analysis**

117 Tentative identification of compounds from *C. gigantea* extracts were carried out using ACQUITY UPLC (Waters
118 Corporation, Milford, MA) system connected to Micromass QTof Premier™ mass spectrometry (Waters
119 Corporation, Milford, MA) with an electrospray ionization device, operating in the negative ion mode, using the
120 following operation parameters: The operation parameters in the negative ion mode were capillary voltage, 2,300
121 V; cone voltage, 50 V; ion source temperature, 110°C; desolvation temperature, 350 °C; flow rate of desolvation
122 gas (N_2), 500 L/h; mass scan range, 100–1500 Da; scan time, 0.25 s. Leucine enkephalin was used as the reference
123 compound (*m/z* 554.2615 in negative ion mode). The gradient elution program was as follows: 0 min, 10% B; 0–
124 1.0 min, 10% B; 1.0–12.0 min, 10–100% B; wash for 13.4 min with 100% B; and a 1.6 min recycle time. The
125 injection volumes were 2.0 μL, and the flow rate was 0.4 mL/min.

126

127 **Cell culture**

128 A549 and NCI-H1299 cells were purchased from the American Type Culture Collection (ATCC: Manassas, VA,
129 USA). Cells were cultured in RPMI 1640 medium (Welgene, Gyeongsan-si, South Korea) containing 10% (v/v)
130 heat-inactivated fetal bovine serum (FBS: Hyclone Laboratories, Logan, UT, USA). Cells were incubated at 37°C
131 in an atmosphere of 5% CO_2/95% air with saturated humidity.

132

133 **Cell viability assays**

134 Cell viability was examined with 3-(4,5-dimethylthiazol-2-yl)-5-(3-carboxymethoxyphenyl)-2-(4-sulfophenyl)-
135 2H-tetrazolium (MTS) assay. A549 cells were seeded at 0.7×10^4 cells and NCI-H1299 cells at 0.9×10^4cells in
136 100 μL medium/well in 96-well plates for overnight growth. After 24 h, various concentrations of CG extract
137 were added, and the cells were incubated for an additional 24 and 48 h. The medium (100 μL) was removed and
138 incubated with 100 μL of MTS with PMS mix solution for 40 min to 1 h at 37°C. The optical densities in each
139 well were measured at 492 nm with an ELISA reader (Apollo LB 9110, Berthold Technologies GmbH, Zug,
140 Switzerland).

141

bioRxiv preprint doi: https://doi.org/10.1101/441162; this version posted October 11, 2018. The copyright holder for this preprint (which was not certified by peer review) is the author/funder, who has granted bioRxiv a license to display the preprint in perpetuity. It is made available under a CC-BY 4.0 International license.

DAPI staining

A549 cells (0.5×10^4 cells) and NCI-H1299 cells (0.7×10^4 cells) were seeded in each well of slide plate and incubated overnight. After that, cells were treated with various concentrations of CG. After 48 h, plates were washed with PBS and cells were fixed with 4 % paraformaldehyde and stained with DAPI staining solution for 10 seconds. The plates were washed with PBS and completely dried. Plates were mounted with cover slip. The stained cells were observed using Fluorescence microscope (Olymous, Tokyo, Japan).

Annexin V/PI staining

A549 cells (1.5×10^5 cells) and NCI-H1299 cells (2.0×10^5 cells) were seeded in 1.5 mL medium/well in 6-well plates for overnight growth. Cells were treated with various concentrations of CG extract for 48 h, harvested using trypsin, and washed with PBS. Annexin V and PI staining were performed using a FITC-Annexin V Apoptosis Detection Kit I (BD Biosciences, San Jose, CA, USA) according to the manufacturer's instructions. Data were analyzed using flow cytometry, employing a FACSCalibur instrument and CellQuest software (BD Biosciences, San Jose, CA, USA).

Cell cycle analysis

The cell cycle distribution was analyzed by PI (propidium iodide) staining and flow cytometry. A549 (1.5×10^5 cells) and NCI-H1299 cells (2.0×10^5 cells) were seeded in 1.5 mL medium/well in 6-well plates for overnight growth and treated with various concentrations of CG extract. After 48 h, cells were harvested with trypsin and fixed with 80% ethanol for > 1 h. Next, the cells were washed twice with cold phosphate-buffered solution (PBS) and centrifuged, and the supernatants were removed. The pellets were re-suspended and stained in PBS containing 50 μg/mL PI and 100 μg/mL RNase A for 20 min in the dark. DNA content was analyzed by flow cytometry using a FACSCalibur instrument and CellQuest software (BD Biosciences, San Jose, CA, USA).

Real-time quantitative polymerase chain reaction (qPCR)

bioRxiv preprint doi: https://doi.org/10.1101/441162; this version posted October 11, 2018. The copyright holder for this preprint (which was not certified by peer review) is the author/funder, who has granted bioRxiv a license to display the preprint in perpetuity. It is made available under a CC-BY 4.0 International license.

A549 cells treated with CG for 48 h were harvested. The harvested cells were lysed in 1 mL easy-BLUE™ (iNtRon Biotechnology, SungNam, Korea). The RNA was isolated according to the manufacturer's instructions. cDNA products were obtained using M-MuL V reverse transcriptase (New England Biolabs, Beverly, MA, USA). Real-time qPCR was performed using a relative quantification protocol using Roter-Gene 6000 series software 1.7 (Qiagen, Venlo, Netherlands) and a SensiFAST™ SYBR NO-ROX Kit (BIOLINE, London, UK). Each sample contained one of the following primer sets: *FAS* F: 5′-CGGACCCAGAATACCAAGTG-3′ and R: 5′-GCCACC CCAAGTTAGATCTG-3′; *FASL F*: 5′-GGGGATGTT TCAGCTCTTCC-3′ and R: 5′-GTGGCCTAT TTG CTT CTCCA-3′; *DR5* F: 5′-CACCTTGTACACGATGC TGA-3′ and R: 5′-GCTCAACAA GTGGTCCTCAA-3′; *FADD* F: 5′-GGGGAAAGATTGGAGAAGGC-3′ and R: 5′-CAGTTCTCAGTGA CTCCCG-3′; *SOD2* F: 5′-TATAGAAAGCCGAGTGTTTCCC-3′ and R: 5′-GGGATGCCTTTC TAGTCCTATTC-3′: *catalase* F: 5′-GGG ATCTTTTAACGCCATT-3′ and R: 5′-CCAGTTTACCAACTGGATG-3′; *thioredoxin* F: 5′-GAAGCTC TGT TTGGTGCTTTG-3′ and R: 5′-CTCGATCTGCTTCACCATCTT-3′ *GAPDH* F: 5′-GGCTGCTTTTAAC TCT GGTA-3′ and R: 5′-TGGAAGATGGTGATGGGATT-3′.

Western blot analysis

A549 cells and NCI-H1299 cells were treated with CG at various concentrations for 48 h, harvested, and then washed with PBS. After centrifugation (13,000 rpm, 1 min, 4°C), the cell pellets were re-suspended in a lysis buffer containing 50 mM Tris (pH 7.4), 1.5 M sodium chloride, 1 mM EDTA, 1% NP-40, 0.25% sodium deoxycholate, 0.1% sodium dodecyl sulfate (SDS), and a protease inhibitor cocktail. The cell lysates were vortexed by a rotator at 4°C for 1 h and clarified by centrifugation at 13,000 rpm for 30 min at 4°C. The protein content was estimated using a Bradford assay (Bio-Rad Laboratories, Hercules, CA, USA) and UV spectrophotometer. The cell lysates were loaded onto a 10–12 % gel and separated by SDS-polyacrylamide gel electrophoresis (PAGE). The protein bands were transferred to polyvinylidene difluoride (PVDF) membranes (Millipore, Billerica, MA, USA). Next, the membranes were blocked with Tris-buffered saline containing Tween-20 (TBST) (2.7 M NaCl, 1M Tris-HCL, 53.65 mM KCL, and 0.1% Tween-20, pH 7.4) and 5% skim milk for 30 min at room temperature. The membranes were incubated overnight at 4°C with primary antibodies targeting specific proteins. After three washes with TBST for 10 min each, the membranes were incubated with a secondary

bioRxiv preprint doi: https://doi.org/10.1101/441162; this version posted October 11, 2018. The copyright holder for this preprint (which was not certified by peer review) is the author/funder, who has granted bioRxiv a license to display the preprint in perpetuity. It is made available under a CC-BY 4.0 International license.

antibody (HRP-conjugated anti-rabbit or anti-mouse IgG) for 2 h at room temperature. After three washes with TBST, the blots were analyzed using West-Zol and a western blot detection system (iNtRON Biotechnology, South Korea).

Nuclear and cytoplasmic fractionation

A549 cells and NCI-H1299 cells treated with CG were collected and fractionated using NE-PER nuclear and cytoplasmic extraction reagents (Thermo Fisher Scientific Inc., USA) according to the manufacturer's instructions. The treated cells were harvested with trypsin-EDTA and centrifuged at 500 × *g* for 3 min. The cell pellets were suspended in 200 μL cytoplasmic extraction reagent I by vortexing. The suspensions were incubated on ice for 10 min, followed by the addition of 11 μL second cytoplasmic extraction reagent II. These reaction mixtures were vortexed for 5 s, incubated in iced for 1 min, and centrifuged at 16,000 × *g* for 5 min. Then, the supernatant fractions were transferred to pre-chilled tubes. The insoluble fractions were resuspended in 100 μL nuclear extraction reagent by vortexing for 15 s. The reaction tubes were incubated on ice for 10 min and centrifuged for 10 min at 16,000 × *g*. The resulting supernatant constituting the nuclear extract was used for subsequent experiments.

Analysis of mitochondrial membrane potential (MMP)

We evaluated MMP ($\Delta\psi m$) by JC-1 staining and flow cytometry. A549 (3.8×10^5 cells) and NCI-H1299 (4.3×10^5 cells) cells were seeded into 3 mL medium/60 mm culture dishes. The cells were treated with various concentrations of CG. Cells were harvested with trypsin-EDTA and transferred into 1.5 mL tubes. JC-1 (5 μg/mL) was added to the cells and mixed until it was completely dissolved, followed by incubation of cells in the dark for 10 min at 37°C in an incubator. The cells were centrifuged (300 × *g*, 5 min, 4°C), washed twice with PBS, and resuspended in 200 μL PBS. The solutions were analyzed using a FACSCalibur instrument and Cell Quest software, in minimal light.

Detection of intracellular levels of ROS

bioRxiv preprint doi: https://doi.org/10.1101/441162; this version posted October 11, 2018. The copyright holder for this preprint (which was not certified by peer review) is the author/funder, who has granted bioRxiv a license to display the preprint in perpetuity. It is made available under a CC-BY 4.0 International license.

We used a DCF-DA cellular ROS detection assay kit (Abcam, UK) to detect the accumulation of intracellular ROS in A549 and NCI-H1299 cells. A549 (0.7×10^4cells) and NCI-H1299 (0.9×10^4cells) cells were seeded into dark 96-well plates and incubated 24 h. The cells were then stained with 25 μM 2′,7′-dichlorofluorescin diacetate (DCF-DA) for 45 min and treated with various concentrations of CG (0, 3.75, 7.5, and 15 μg/mL) for 48 h. The fluorescence intensity of each well was quantified with a fluorescence microplate reader (Gemini EM, Molecular Devices, USA) at excitation/emission = 485/538 nm. The experiments were performed at least three times.

Results

Tentative identification of phytochemicals in CG

UPLC-PDA-QTof-MS analyses were carried out using a C18 column with a linear gradient of acetonitrile/water (Fig. 1). All peaks were characterized using Mass. Table 1 shows the retention times, UV–Vis absorption maxima, mass spectral data of molecular ions of these compounds in the CG extract, namely quercetin 3-rutinoside, kaempferol-4′-O-rutinoside, kaempferol-3-O-rutinoside, isorhamnetin-3-O-rutinoside, deglucoerycordin, 15ß-hydroxycalotropin, frugoside, and trihydroxy octadecenoic acid. Various rutinosides and a high level of isorhamnetin-3-O-rutinoside, particularly, were found in the CG extract.

Figure 1. Representative UPLC-QTof-MS chromatograms of the methanol extracts from CG. Peak numbers refer to Table 1. The composition of CG was analyzed by UPLC-QTof-MS. Among the compounds in CG, isorhamnetin-3-O-rutinoside was a major component.

bioRxiv preprint doi: https://doi.org/10.1101/441162; this version posted October 11, 2018. The copyright holder for this preprint (which was not certified by peer review) is the author/funder, who has granted bioRxiv a license to display the preprint in perpetuity. It is made available under a CC-BY 4.0 International license.

240 **Table 1. Quantitative HPLC analyses of composition in CG extraction.**

Peak	ESI-MS RT(min)	UV (nm)	Detected ion (m/z)	Calculated ion (m/z)	Error (ppm)	MS-MS ions (m/z)	Tentative identification	Molecular formula
1	3.17	208, 254, 352	609.1424	609.1456	-5.3	179, 300, 301	Quercetin 3-rutinoside	$C_{27}H_{30}O_6$
2	3.35	208, 265, 344	593.1505	593.1506	-0.2	179, 284	Kaempferol-4'-O-rutinoside	$C_{27}H_{30}O_{15}$
3	3.45	203, 254, 352	593.1472	593.1506	-5.7	151, 179, 285	Kaempferol-3-O-rutinoside	$C_{27}H_{30}O_{15}$
4	3.52	203, 254, 353	623.1595	623.1612	-2.7	179, 315, 593	Isorhamnetin-3-O-rutinoside	$C_{28}H_{32}O_{16}$
5	3.84	219	697.3453	697.3470	-2.4	389, 535	Deglucoerycordin	$C_{35}H_{54}O_{14}$
6	4.21	225	547.2565	547.2543	4.0	179, 343, 401, 419	15b-hydroxycalotropin	$C_{28}H_{40}O_{10}$
7	4.42	225	535.2933	535.2907	0.7	179, 389	Frugoside	$C_{29}H_{44}O_5$
8	5.62	225	329.2387	329.2328	5.9	171, 206, 211	Trihydroxy octadecenoic acid	$C_{18}H_{34}O_5$

241

242

243 **CG induces cytotoxic effects in human NSCLC cells**

244 Several studies have been reported on the effects of plant extracts inhibiting tumor growth, metastasis, and
245 angiogenesis [18]. This study was aimed to determine whether CG could induce cytotoxicity, examined in A549
246 and NCI-H1299 cells following treatment with various concentrations (up to 15 μg/ml for 24 and 48 h) of CG.
247 The MTS assay showed that the cell viability rate declined in a dose-dependent manner by CG (Fig. 2A and B).
248 The viabilities of A549 and NCI-H1299 cells treated with the highest (up to 15 μg/ml) CG concentrations at 48 h
249 were both less than 50% that in DMSO (0.01%) treated control cells; the viabilities of A549 and NCI-H1299 cells
250 treated with CG decreased significantly after 48 h. Therefore, CG extract was found to exert cytotoxic effects on
251 lung cancer cells. Thus, our next study was focused on verifying the mechanism underlying NSCLC apoptosis
252 following up to 15 μg/ml of CG for 48 h on NSCLC cells.

253

254 **Figure 2. Cytotoxic effects of CG extract on human NSCLC cell lines.** The viabilities of A549 (A) and NCI-
255 H1299 cells (B). A549 and NCI-H1299 cells were treated for 24 and 48 h with CG extract. The untreated cells
256 were compared with CG-treated cells. Results with $*p < 0.05$ and $**p < 0.005$ were considered statistically

bioRxiv preprint doi: https://doi.org/10.1101/441162; this version posted October 11, 2018. The copyright holder for this preprint (which was not certified by peer review) is the author/funder, who has granted bioRxiv a license to display the preprint in perpetuity. It is made available under a CC-BY 4.0 International license.

significant. Viability was analyzed by MTS assay.

CG induces apoptosis in A549 and NCI-H1299 lung cancer cells

As the viabilities of A549 and NCI-H1299 cells treated with CG decreased dose dependently, cell morphological changes were observed by phase-contrast microscopy. As expected, these morphological changes were dependent on the dose of CG extract used to treat cells for 48 h. A549 (Fig. 3A) and NCI-H1299 (Fig. 3B) cells morphologies became more rounded and less interactions with surrounding cells were observed at high concentrations of CG than in DMSO (0.01%) treated control cells. This indicated that CG can change cell morphology, subsequently inducing cell death [19]. DAPI staining and fluorescence microscopy showed that CG-treated A549 cells (Fig. 3C) and NCI-H1299 cells (Fig. 3D) had condensed and their nuclei had fragmented—a marker of apoptosis—relative to the control cells. For further evidence of the effects of CG, CG treated A549 and NCI-H1299 cells were examined by Annexin V and PI staining [20]. When apoptosis occurs in the cells, lipid phosphatidylserine (PS) in the membranes of cells is translocated from the inner to the outer membrane, a so-called flip-flop movement, and Annexin V staining targets the PS [20]. Furthermore, the cell membranes had pores that facilitated apoptosis mediated via PI binding to DNA. The Annexin V- FITC/ PI staining indicated apoptosis in A549 (Fig. 3E) and NCI-H1299 cells (Fig. 3F) following treatment with CG extract. Cells of both types treated with CG for 48 h revealed increasing numbers of early and late apoptotic cells, whereas the number of live cells decreased. In A549 cells, the number of late apoptotic cells increased up to 35.30% with 15 µg/mL of CG treatment compared to that in control cells, 6.75 %. The rate of increase (3.42 % to 13.07 %) of late apoptotic cells among all NCI-H1299 cells was lesser than that of A549 cells. These results indicated that the death of A549 and NCI-H1299 cells induced by CG extract was thus mediated by apoptosis.

Figure 3. Effects of CG on viability and apoptosis in A549 and NCI-H1299 lung cancer cells. Microscopic images of A549 (A) and NCI-H1299 cells (B) treated with CG for 48 h. Fluorescence microscopic images showed that nuclear condensation and chromatin shrinkage were apparent in A549 (C) and NCI-H1299 cells (D) treated with CG for 48 h. After treatment with the indicated concentrations of CG for 48 h, A549 (E) and NCI-H1299 cells (F) were stained with Annexin V-FITC/PI. Untreated cells were compared with CG-treated cells.

bioRxiv preprint doi: https://doi.org/10.1101/441162; this version posted October 11, 2018. The copyright holder for this preprint (which was not certified by peer review) is the author/funder, who has granted bioRxiv a license to display the preprint in perpetuity. It is made available under a CC-BY 4.0 International license.

CG modulates cell cycle-related factors in A549 cells and controls cell cycle progression in A549 and NCI-H1299 cells

Cell cycle disruption is a major cause of apoptosis in cancer calls [21], and many factors such as p53, p27, p21, and cyclins control cell cycle phases. p53 is known as a tumor suppressor gene [22]. When DNA has been damaged, it is activated to induce apoptosis. In addition, phosphorylated p53, p27 and p21, downstream factors of p53, regulate cyclin dependent kinase. The levels of p53 in A549 cells following treatment with 7.5 μg/mL and 15 μg/mL of CG extract were increased compared to that of the control, and 3.75 (μg/mL) concentrations and p27 was upregulated by CG as same as p53, but p21 was not (Fig. 4A). This suggests that p53 and p27 were stimulated by CG and induced the death of A549 cells by terminating the cell cycle. However, in NCI-H1299 p53-knockout cells, the cell cycle regulatory factors p27 and p21 were not affected by CG treatment (Fig. 4B). The cell cycle analyses of CG treated A549 (Fig. 4C) and NCI-H1299 cells (Fig. 4D) were performed by flow cytometry. Cells in the sub-G1 phase showed fragmented DNA, which is a marker of apoptosis [23, 24]. In our study, the cell cycle analysis showed that cells in the sub-G1 phase and S phase increased in a dose-dependent manner with CG treatment for A549 cells (Fig. 4E) and NCI-H1299 cells (Fig. 4F), whereas cells in the G0/G1 and G2/M phases decreased for both cell line. Furthermore, the cell cycle related factors cyclin D1 related to the sub-G1 phase and cyclin A related to the S phase, were downregulated as expected, but cyclin E in A549 cells was not altered by CG treatment (Fig. 4G). However, the levels of cyclin D1, E, and A decreased with treatment of NCI-H1299 cells (Fig. 4H). These results indicated that CG extract had negative effects on the A549 and NCI-H1299 cell cycles, reducing the restrictions against unlimited cell growth.

Figure 4. Effects of CG on p53-dependent apoptotic signaling in A549 cells and on the cell cycle phases in A549 and NCI-H1299 lung cancer cells. (A) Protein expression levels of p53, p27, p21, and GAPDH in A549 cells and (B) protein expression levels of p27, p21, and GAPDH in NCI-H1299 cells as determined by western blot analyses. A549 and NCI-H1299 cells were treated with various concentrations of CG for 48 h and compared with untreated cells. Cell cycle profiles of CG-treated A549 (C) and NCI-H1299 cells (D). The cells were treated with CG for 48 h, fixed, and stained with PI. A549 (E) and NCI-H1299 cells (F) in the sub-G1 phase. Results with

bioRxiv preprint doi: https://doi.org/10.1101/441162; this version posted October 11, 2018. The copyright holder for this preprint (which was not certified by peer review) is the author/funder, who has granted bioRxiv a license to display the preprint in perpetuity. It is made available under a CC-BY 4.0 International license.

311 $^{**}p < 0.005$ were considered statistically significant. Protein expression levels of cyclin D1, cyclin E, cyclin A,
312 and GAPDH in A549 (G) and NCI-H1299 cells (H) as determined by western blot analyses.

313

314 **CG induces the extrinsic pathway of apoptosis by activating death receptors and downregulating signaling**

315 The extrinsic pathway of apoptosis is the other important pathway leading to apoptosis [25]. This pathway is
316 distinct from the intrinsic pathway. The interactions between ligands and death receptors promote the formation
317 of a death-inducing signaling complex (DISC), and caspase-8 is activated [26]. To confirm the mRNA levels of
318 extrinsic pathway factors, real-time qPCR was performed. The results showed that factors in the extrinsic pathway
319 tended to increase. The mRNA expression levels of death receptor 5 (DR5), FADD, FAS, and FASL were
320 increased in CG-treated A549 (Fig. 5A) and NCI-H1299 cells (Fig. 5C). Furthermore, the pro-forms of caspase-
321 8 expression levels decreased in a CG dose-dependent manner, and cleaved forms appeared following treatment
322 with high concentrations of CG in A549 cells (Fig. 5B) and NCI-H1299 cells (Fig. 5D). These results
323 demonstrated that CG was effective in inducing cell death through the process of apoptosis in A549 and NCI-
324 H1299 lung cancer cells.

325

326 **Figure 5. Effects of CG on extrinsic pathway-related factors in A549 and NCI-H1299 cells.** mRNA levels of
327 DR5, FADD, FAS, and FASL in A549 (A) and NCI-H1299 cells (C) as determined by qPCR. The graph was
328 compiled from at least three replicates. Protein expression levels of the extrinsic pathway factors, pro-caspase-8
329 and its cleaved form, in A549 (B) and NCI-H1299 cells (D) as determined by western blot analyses. Cells were
330 treated with various concentrations of CG for 48 h and compared with untreated cells. Results with $^{*}p < 0.05$ and
331 $^{**}p < 0.005$ were considered statistically significant.

332

333 **CG has an apoptotic effect on mitochondrial and intracellular downregulation signals**

334 The extrinsic and intrinsic pathways of apoptosis cross at the level of the mitochondria [27]. Activated caspase-8
335 cleaves the protein Bid into tBid, which is an activated form. This is mediated by members of the Bcl-2 family.
336 tBid induces Bax-dependent outer mitochondrial membrane permeabilization and the release of cytochrome c [28].

bioRxiv preprint doi: https://doi.org/10.1101/441162; this version posted October 11, 2018. The copyright holder for this preprint (which was not certified by peer review) is the author/funder, who has granted bioRxiv a license to display the preprint in perpetuity. It is made available under a CC-BY 4.0 International license.

Bid expression level was decreased, while Bax was enhanced in A549 cells following treatment with CG (Fig. 6A). Bcl-2, which is an inhibitory factor in the intrinsic pathway of apoptosis, also decreased, but the levels of Bcl-xL were not altered. These levels were similar in NCI-H1299 and A549 cells (Fig. 6E). Thus, Bax stimulated by Bid and Bcl-2 controlled MMP. The fluorescence of cells stained with JC-1 change from orange to green when apoptosis is in progress and MMP is decreasing. The orange fluorescence of A549 cells (Fig. 6B) and NCI-H1299 cells (Fig. 6F) exhibited a dose-dependent leftward shift following treatment with CG. Moreover, cytochrome c from mitochondrial membranes appeared in the cytosol in CG-treated A549 cells (Fig. 6C) and NCI-H1299 cells (Fig. 6G) as determined by western blot. Mitochondrion dysfunction is a very important signal in the intrinsic pathway of apoptosis [27], and mitochondria membrane collapse caused caspase-9 to be released. This study confirmed that factors such as caspase-9 and caspase-3, which are controlled by members of the Bcl-2 family (e.g., Bcl-2 and Bcl-xL) [29] decreased and were cleaved to induce apoptosis in a dose-dependent manner following CG treatment of A549 cells (Fig. 6D) and NCI-H1299 cells (Fig. 6H) as determined by western blot assay. The cleaved forms of these proteins were found following treatment at the highest concentration of CG in both cell lines. This suggests that these cleaved forms activated apoptosis. Finally, the key factor in programmed cell death and DNA repair, PARP, was cleaved by CG in the two types of cells (Fig. 6D and H). These results indicated CG-induced apoptosis following signaling in the intrinsic pathway.

Figure 6. Effects of CG on MMP and intrinsic pathway-related factors in A549 and NCI-H1299 cells. Protein expression levels of BID, Bcl-2, Bcl-xL, BAX, and GAPDH in A549 (A) and NCI-H1299 cells (E) as determined by western blots. Cells were treated with various doses of CG extract for 48 h and compared with untreated cells. Histogram profiles of JC-1 aggregates (FL-2, orange) detected by flow cytometry of A549 (B) and NCI-H1299 cells (F). Western blots of cytochrome c protein levels in membranes and cytosol fractions and GAPDH in A549 (C) and NCI-H1299 cells (G). Cells were fractionated using an NE-PER nuclear cytoplasmic extraction reagent kit (Thermo, USA). Protein levels of the intrinsic pathway factors, caspase-9, caspase-3, PARP, and GAPDH in A549 (D) and NCI-H1299 cells (H) as determined by western blot analyses.

CG generates ROS products

bioRxiv preprint doi: https://doi.org/10.1101/441162; this version posted October 11, 2018. The copyright holder for this preprint (which was not certified by peer review) is the author/funder, who has granted bioRxiv a license to display the preprint in perpetuity. It is made available under a CC-BY 4.0 International license.

364 To determine how apoptosis occurs in p53-independent death of NCI-H1299 cells, we examined the generation
365 of ROS, which is a main cause of apoptosis [23, 30]. There are many studies on ROS related to apoptosis. ROS
366 levels can increase dramatically with environmental stress and result in significant damage called oxidative stress
367 [5]. Therefore, we investigated the effect of CG on ROS production in A549 and NCI-H1299 cells. First, we
368 examined ROS levels in A549 and NCI-H1299 cells treated with CG. After CG treatment for 48 h, these cells
369 were stained with 2′,7′-dichlorofluorescin diacetate (DCF-DA), and the amount of ROS produced was determined
370 by fluorescence microscopy. ROS accumulated dose dependently in A549 cells (Fig. 7A) and NCI-H1299 cells
371 (Fig. 7C) following treatment with CG. Furthermore, ROS scavengers that had an anti-apoptotic role, superoxide
372 dismutase 2 (SOD2) and catalase, decreased in A549 cells (Fig. 7B) and NCI-H1299 cells (Fig. 7D) in response
373 to CG, but levels of the other ROS scavenger, thioredoxin (TXN), were unaltered (Fig. 7B and D). This study
374 suggests that generated ROS might trigger or at least be implicated in CG-induced apoptosis.

375

376 **Figure 7. CG induced ROS generation in A549 and NCI-H1299 cells.** CG treatment resulted in ROS generation
377 in A549 (A) and NCI-H1299 cells (C). Cells were treated with CG for 48 h and examined using DCFDA
378 fluorescence staining and a fluorescence microplate reader. The mRNA levels of superoxide dismutase (SOD2),
379 catalase, thioredoxin (TXN), and GAPDH were determined by qPCR in A549 (B) and NCI-H1299 cells (D)
380 treated with CG extract for 48 h. Results with $*p < 0.05$ and $**p < 0.005$ were considered statistically significant.

381

382 **ROS scavenger N-acetylcysteine (NAC) recovers cell viability**

383 To confirm that CG extract induced apoptosis mediated by ROS generation, we used the ROS scavenger N-
384 acetylcysteine (NAC) [23, 31] and examined cell viability and ROS generation. A549 and NCI-H1299 cells were
385 pre-treated with NAC, and cell viability was confirmed. Cell viabilities dramatically recovered to over 100% in
386 CG and NAC treatment groups, compared with the viabilities in the CG-treated groups of A549 cells (Fig. 8A)
387 and NCI-H1299 cells (Fig. 8B). ROS generation levels also decreased with CG and NAC treatment of A549 (Fig.
388 8C) and NCI-H1299 cells (Fig. 8D), compared to the levels in CG-treated cells. Collectively, these results
389 indicated that CG exerted anti-lung cancer effects through ROS-mediated apoptosis and the inhibition of ROS

bioRxiv preprint doi: https://doi.org/10.1101/441162; this version posted October 11, 2018. The copyright holder for this preprint (which was not certified by peer review) is the author/funder, who has granted bioRxiv a license to display the preprint in perpetuity. It is made available under a CC-BY 4.0 International license.

390 generation, which sufficiently blocked CG-induced apoptosis.

391 **Figure 8. ROS scavenger N-acetylcysteine (NAC) recovered the cell viability and attenuated ROS production**
392 **in CG-treated A549 and NCI-H1299 cells.** Pre-treated NAC recovered the cell viability of A549 (D) and NCI-H1299
393 cells (B). A549 (C) and NCI-H1299 cells (D) were pretreated with NAC and then treated CG for 48 h. Then, the cells
394 were stained with DCF-DA and examined using a fluorescence microplate reader. Results with *$p < 0.05$ and **$p <$
395 0.005 were considered statistically significant.

396

397

398 **Discussion**

399 Many plant extracts are known as significant potential about anticancer effects [23, 32] such as inhibition of
400 tumor growth, angiogenesis and metastasis. CG is one of plant extracts and few reports studied about the
401 antiproliferative effects of the plant.

402 First, we analyzed that the chemical compounds of CG extract and the diverse rutinosides, well-known effective
403 anti-cancer chemical [33], were detected. Among them, isorhamnetin-3-O-rutinoside which included high amount in
404 CG extract has been investigated the apoptosis of human myelogenous erythroleukaemia cells [34], but had no effect
405 about cytotoxicity in NSCLC cells (Fig. S1 in Supporting Information). However, CG extract has cytotoxic effects
406 in non-small-cell lung cancer cells, especially in A549 (p53+/+) cells and NCI-H1299 (p53-/-) cells [35]. Not only
407 cells' morphology of the A549 cells and NCI-H1299 cells changed to more round shape and less cell-cell
408 interaction than untreated cells as previous reported [36], but also the nuclear of both cells were fragmented and
409 shrunk with CG treatment. Also, the late apoptosis was increased in a dose dependent CG treated A549 cells and
410 NCI-H1299 cells. It meant that the cytotoxicity of these cells was because of apoptotic effects of CG extract.

411 p53 is well known as a tumor suppressor protein [22] and it stimulates the downstream factor, p27 [37]. p27 has
412 ability to control the cell cycle which regulates cyclin D, the growth stimulation protein of the cyclin family [38].
413 Cyclin family such as cyclin D1, E, and A is involved in each specific phases of the cell cycle. During the cell
414 cycle, hypodiploid fragmented DNA [21], one of apoptotic marker, is existed in Sub-G1 phage. In this study, p53
415 null NCI-H1299 cells were also used. As shown in Fig. 2B, the cytotoxicity of CG in NCI-H1299 cells was
416 presented and it meant that CG extract induced cell death independent of p53 in NCI-H1299 cells. However, we

bioRxiv preprint doi: https://doi.org/10.1101/441162; this version posted October 11, 2018. The copyright holder for this preprint (which was not certified by peer review) is the author/funder, who has granted bioRxiv a license to display the preprint in perpetuity. It is made available under a CC-BY 4.0 International license.

417 confirmed that the expression levels of p53 and phospho-p53 (pp53) were increased in A549 cells (wild type
418 p53+/+), treated with CG. As shown in Fig. 3E and 3F, the increasing rate of late apoptosis in NCI-H1299 cells
419 was less than in A549 cells. These results demonstrated that p53 was strongly related to apoptosis, so p53
420 stimulated by CG in A549 cells induced a crucial apoptosis in compared to NCI-H1299 cells. Hence, p53 was one
421 of essential factors to cause cytotoxic effect of CG in A549 cells. Also, p27 level was increase and controlled the
422 cell cycle in A549 cells. During the cell cycle of the A549 cells and NCI-H1299 cells treated with CG, sub-G1
423 phase and S phage were increased, and G0/G1 phase population was decreased [23, 39]. It meant that the number
424 of hypodiploid fragmented DNA in subG1 phage was increased and the cell cycle was limited by CG. Cyclin D1,
425 a major player to activate G1 phase of cell cycle, was marginally inhibited and in S phage, cyclin A related to
426 DNA replication [40] was decreased by CG in A549 cells and NCI-H1299 cells. In NCI-H1299 cells, cyclin E
427 related to DNA replication, was also decreased by CG. Thus, it showed that CG extract caused adverse effects in
428 the cell cycle of A549 cells and NCI-H1299 cells to stop the cells' growth and induced apoptosis.

429 Apoptosis is elimination of damaged cells through ordered cell death system [6, 23]. There are two main
430 pathways of apoptosis; extrinsic pathway and intrinsic pathway. We investigated that CG treatment increased the
431 ratio of the death receptors, death ligands, adaptors and DISC of extrinsic pathway in A549 cells and NCI-H1299
432 cells. Also, extrinsic pathway and intrinsic pathway were connected through increased Bcl-2 and Bax by CG.
433 Continuously, intrinsic programmed cell death by mitochondria outer membrane permeabilization (MOMP) [28]
434 was induced and cytochrome c was released from mitochondria into the cytoplasm. This stimulation occurs
435 downstream signaling cascade that cleaves other intrinsic caspases and PARP resulting in apoptosis [10, 23] by
436 CG in both cells. CG extract induced apoptosis by stimulating the receptors and ligands of extrinsic pathway in
437 A549 cells and NCI-H1299 cells. Additionally, the significant factors inducing the apoptotic intrinsic pathway in
438 CG-treated A549 cells and NCI-H1299 cells were detected. It meant that CG induced apoptosis was depend on
439 both pathways of intrinsic and extrinsic signaling in NSCLC.

440 There are numbers of evidences emphasizing the principal role of reactive oxidase species (ROS) production
441 which induce cell death in various cancer cell types [13, 23]. Recent studies show that anticancer agents mediate
442 their apoptotic effects through ROS and the ROS production is prevented by ROS scavenger blocking cell death
443 [31]. In agreement with these studies, we observed CG-enhanced ROS generation in A549 and NCI-H1299 lung
444 cancer cells in a dose dependent manner. Furthermore, the cell viabilities and ROS generation levels were

bioRxiv preprint doi: https://doi.org/10.1101/441162; this version posted October 11, 2018. The copyright holder for this preprint (which was not certified by peer review) is the author/funder, who has granted bioRxiv a license to display the preprint in perpetuity. It is made available under a CC-BY 4.0 International license.

445 recovered with the ROS scavenger, N-acetylcysteine (NAC), in A549 cells and NCI-H1299 cells.

446 In conclusion, CG has a cytotoxic effect against non-small lung cancer cells and inhibits via not only p53
447 dependent pathway in A549 cells but also p53 independent pathway in NCI-H1299 cells. This signaling is related
448 with cell cycle through p27 in A549 cells. During cell cycle, the sub-G1 populations were increased with
449 downregulation of cyclin D1 and cyclin A is decreased in A549 cells and NCI-H1299 cells. Also, cyclin E
450 expression was controlled by CG in NCI-H1299 cells. Notably, CG induces the extrinsic and intrinsic apoptotic
451 pathway mediated by death receptors, cytochrome c and caspases and inactivated by PARP through controlling
452 Bcl-2 and Bax in A549 cells and H199 cells. CG also enhances ROS level and a ROS scavenger, NAC, recovers
453 reduced cell viability by CG in A549 cells and NCI-H1299 cells. To summarize, CG plant extract has a profound
454 anti-cancer effect and these experiments strongly support the apoptotic effects (Fig. 9). Through *in vivo*
455 experiments in future study, the plants extract, CG, can be developed and used in lung cancer therapy.

456

457 **Figure 9. Schematic diagram illustrating CG-induced apoptotic effects in human NSCLC cell lines.** CG
458 triggers death receptor (DR5 and FAS)- and adaptor (FADD)-mediated apoptotic signaling pathways, as well as
459 caspase-8 processing, resulting in cytochrome c release that is regulated by Bcl-2, Bid, and Bax. Subsequently,
460 activated caspase-9 followed by caspase-3 cleaves PARP, resulting in triggering apoptosis. Moreover, CG induces
461 apoptosis through ROS generation by controlling the ROS scavengers such as catalase and SOD2 in mitochondria.
462 CG stimulates tumor suppressor p53 and cyclin-dependent kinase inhibitor p27. Cell cycle is also suppressed by
463 a reduction in cyclin factors.

464

465

466 **Acknowledgements**

467 This research was supported by Konkuk University in 2018.

468

bioRxiv preprint doi: https://doi.org/10.1101/441162; this version posted October 11, 2018. The copyright holder for this preprint (which was not certified by peer review) is the author/funder, who has granted bioRxiv a license to display the preprint in perpetuity. It is made available under a CC-BY 4.0 International license.

469 **References**

470

471 1. Cavallo F, De Giovanni C, Nanni P, Forni G, Lollini PL. 2011: the immune hallmarks of cancer.
472 Cancer Immunol Immunother. 2011;60(3):319-26. doi: 10.1007/s00262-010-0968-0. PubMed PMID:
473 21267721; PubMed Central PMCID: PMCPMC3042096.
474 2. Kenfield SA, Wei EK, Stampfer MJ, Rosner BA, Colditz GA. Comparison of aspects of
475 smoking among the four histological types of lung cancer. Tobacco control. 2008;17(3):198-204.
476 doi: 10.1136/tc.2007.022582. PubMed PMID: 18390646; PubMed Central PMCID: PMC3044470.
477 3. Paone G, De Angelis G, Portalone L, Greco S, Giosue S, Taglienti A, et al. Validation of an
478 algorithm able to differentiate small-cell lung cancer (SCLC) from non-small-cell lung cancer (NSCLC)
479 patients by means of a tumour marker panel: analysis of the errors. Br J Cancer. 1997;75(3):448-50.
480 PubMed PMID: 9020496; PubMed Central PMCID: PMCPMC2063371.
481 4. Lee ER, Kang YJ, Choi HY, Kang GH, Kim JH, Kim BW, et al. Induction of apoptotic cell death
482 by synthetic naringenin derivatives in human lung epithelial carcinoma A549 cells. Biol Pharm Bull.
483 2007;30(12):2394-8. PubMed PMID: 18057732.
484 5. Ou L, Lin S, Song B, Liu J, Lai R, Shao L. The mechanisms of graphene-based materials-
485 induced programmed cell death: a review of apoptosis, autophagy, and programmed necrosis. Int
486 J Nanomedicine. 2017;12:6633-46. doi: 10.2147/IJN.S140526. PubMed PMID: 28924347; PubMed
487 Central PMCID: PMCPMC5595361.
488 6. de Bruin EC, Medema JP. Apoptosis and non-apoptotic deaths in cancer development and
489 treatment response. Cancer Treat Rev. 2008;34(8):737-49. doi: 10.1016/j.ctrv.2008.07.001. PubMed
490 PMID: 18722718.
491 7. Wei MC, Zong WX, Cheng EH, Lindsten T, Panoutsakopoulou V, Ross AJ, et al. Proapoptotic
492 BAX and BAK: a requisite gateway to mitochondrial dysfunction and death. Science.
493 2001;292(5517):727-30. doi: 10.1126/science.1059108. PubMed PMID: 11326099; PubMed Central
494 PMCID: PMCPMC3049805.
495 8. Ottilie S, Diaz JL, Horne W, Chang J, Wang Y, Wilson G, et al. Dimerization properties of
496 human BAD. Identification of a BH-3 domain and analysis of its binding to mutant BCL-2 and BCL-XL
497 proteins. J Biol Chem. 1997;272(49):30866-72. PubMed PMID: 9388232.
498 9. Yuan S, Akey CW. Apoptosome structure, assembly, and procaspase activation. Structure.
499 2013;21(4):501-15. doi: 10.1016/j.str.2013.02.024. PubMed PMID: 23561633; PubMed Central PMCID:
500 PMCPMC3644875.
501 10. Chaitanya GV, Steven AJ, Babu PP. PARP-1 cleavage fragments: signatures of cell-death
502 proteases in neurodegeneration. Cell Commun Signal. 2010;8:31. doi: 10.1186/1478-811X-8-31.
503 PubMed PMID: 21176168; PubMed Central PMCID: PMCPMC3022541.
504 11. Walczak H. Death receptor-ligand systems in cancer, cell death, and inflammation. Cold

bioRxiv preprint doi: https://doi.org/10.1101/441162; this version posted October 11, 2018. The copyright holder for this preprint (which was not certified by peer review) is the author/funder, who has granted bioRxiv a license to display the preprint in perpetuity. It is made available under a CC-BY 4.0 International license.

505 Spring Harb Perspect Biol. 2013;5(5):a008698. doi: 10.1101/cshperspect.a008698. PubMed PMID:
506 23637280; PubMed Central PMCID: PMCPMC3632055.
507 12. Holdenrieder S, Stieber P. Circulating apoptotic markers in the management of non-small
508 cell lung cancer. Cancer Biomark. 2010;6(3-4):197-210. doi: 10.3233/CBM-2009-0130. PubMed PMID:
509 20660965.
510 13. Schieber M, Chandel NS. ROS function in redox signaling and oxidative stress. Curr Biol.
511 2014;24(10):R453-62. doi: 10.1016/j.cub.2014.03.034. PubMed PMID: 24845678; PubMed Central
512 PMCID: PMCPMC4055301.
513 14. Mates JM, Sanchez-Jimenez FM. Role of reactive oxygen species in apoptosis: implications
514 for cancer therapy. Int J Biochem Cell Biol. 2000;32(2):157-70. PubMed PMID: 10687951.
515 15. Hockenbery DM, Oltvai ZN, Yin XM, Milliman CL, Korsmeyer SJ. Bcl-2 functions in an
516 antioxidant pathway to prevent apoptosis. Cell. 1993;75(2):241-51. PubMed PMID: 7503812.
517 16. Cai J, Jones DP. Superoxide in apoptosis. Mitochondrial generation triggered by
518 cytochrome c loss. J Biol Chem. 1998;273(19):11401-4. PubMed PMID: 9565547.
519 17. Rathod NR, Chitme HR, Irchhaiya R, Chandra R. Hypoglycemic Effect of Calotropis gigantea
520 Linn. Leaves and Flowers in Streptozotocin-Induced Diabetic Rats. Oman Med J. 2011;26(2):104-8.
521 doi: 10.5001/omj.2011.26. PubMed PMID: 22043394; PubMed Central PMCID: PMCPMC3191672.
522 18. Chen Y, Zhu J, Zhang W. Antitumor effect of traditional Chinese herbal medicines against
523 lung cancer. Anticancer Drugs. 2014;25(9):983-91. doi: 10.1097/CAD.0000000000000127. PubMed
524 PMID: 24892722.
525 19. Ren ZX, Yu HB, Li JS, Shen JL, Du WS. Suitable parameter choice on quantitative
526 morphology of A549 cell in epithelial-mesenchymal transition. Biosci Rep. 2015;35(3). doi:
527 10.1042/BSR20150070. PubMed PMID: 26182364; PubMed Central PMCID: PMCPMC4613694.
528 20. van Engeland M, Nieland LJ, Ramaekers FC, Schutte B, Reutelingsperger CP. Annexin V-
529 affinity assay: a review on an apoptosis detection system based on phosphatidylserine exposure.
530 Cytometry. 1998;31(1):1-9. PubMed PMID: 9450519.
531 21. Meikrantz W, Schlegel R. Apoptosis and the cell cycle. J Cell Biochem. 1995;58(2):160-74.
532 doi: 10.1002/jcb.240580205. PubMed PMID: 7673324.
533 22. Porebska I, Sobanska E, Kosacka M, Jankowska R. Apoptotic regulators: P53 and survivin
534 expression in non-small cell lung cancer. Cancer Genomics Proteomics. 2010;7(6):331-5. PubMed
535 PMID: 21156966.
536 23. Kwon T, Bak Y, Park YH, Jang GB, Nam JS, Yoo JE, et al. Peroxiredoxin II Is Essential for
537 Maintaining Stemness by Redox Regulation in Liver Cancer Cells. Stem Cells. 2016;34(5):1188-97.
538 doi: 10.1002/stem.2323. PubMed PMID: 26866938.
539 24. Kajstura M, Halicka HD, Pryjma J, Darzynkiewicz Z. Discontinuous fragmentation of nuclear
540 DNA during apoptosis revealed by discrete "sub-G1" peaks on DNA content histograms. Cytometry
541 A. 2007;71(3):125-31. doi: 10.1002/cyto.a.20357. PubMed PMID: 17252584.

bioRxiv preprint doi: https://doi.org/10.1101/441162; this version posted October 11, 2018. The copyright holder for this preprint (which was not certified by peer review) is the author/funder, who has granted bioRxiv a license to display the preprint in perpetuity. It is made available under a CC-BY 4.0 International license.

542 25. Elmore S. Apoptosis: a review of programmed cell death. Toxicol Pathol. 2007;35(4):495-
543 516. doi: 10.1080/01926230701320337. PubMed PMID: 17562483; PubMed Central PMCID:
544 PMCPMC2117903.
545 26. Munoz-Pinedo C, Lopez-Rivas A. A role for caspase-8 and TRAIL-R2/DR5 in ER-stress-
546 induced apoptosis. Cell Death Differ. 2018;25(1):226. doi: 10.1038/cdd.2017.155. PubMed PMID:
547 28984868; PubMed Central PMCID: PMCPMC5729524.
548 27. Wang C, Youle RJ. The role of mitochondria in apoptosis*. Annu Rev Genet. 2009;43:95-
549 118. doi: 10.1146/annurev-genet-102108-134850. PubMed PMID: 19659442; PubMed Central PMCID:
550 PMCPMC4762029.
551 28. Zhang M, Zheng J, Nussinov R, Ma B. Release of Cytochrome C from Bax Pores at the
552 Mitochondrial Membrane. Sci Rep. 2017;7(1):2635. doi: 10.1038/s41598-017-02825-7. PubMed PMID:
553 28572603; PubMed Central PMCID: PMCPMC5453941.
554 29. Gibson CJ, Davids MS. BCL-2 Antagonism to Target the Intrinsic Mitochondrial Pathway of
555 Apoptosis. Clin Cancer Res. 2015;21(22):5021-9. doi: 10.1158/1078-0432.CCR-15-0364. PubMed
556 PMID: 26567361; PubMed Central PMCID: PMCPMC4646729.
557 30. Simon HU, Haj-Yehia A, Levi-Schaffer F. Role of reactive oxygen species (ROS) in apoptosis
558 induction. Apoptosis. 2000;5(5):415-8. PubMed PMID: 11256882.
559 31. Halasi M, Wang M, Chavan TS, Gaponenko V, Hay N, Gartel AL. ROS inhibitor N-acetyl-L-
560 cysteine antagonizes the activity of proteasome inhibitors. Biochem J. 2013;454(2):201-8. doi:
561 10.1042/BJ20130282. PubMed PMID: 23772801; PubMed Central PMCID: PMCPMC4322432.
562 32. Solowey E, Lichtenstein M, Sallon S, Paavilainen H, Solowey E, Lorberboum-Galski H.
563 Evaluating medicinal plants for anticancer activity. ScientificWorldJournal. 2014;2014:721402. doi:
564 10.1155/2014/721402. PubMed PMID: 25478599; PubMed Central PMCID: PMCPMC4248331.
565 33. Chen YC, Shen SC, Lin HY. Rutinoside at C7 attenuates the apoptosis-inducing activity of
566 flavonoids. Biochem Pharmacol. 2003;66(7):1139-50. PubMed PMID: 14505793.
567 34. Boubaker J, Bhouri W, Ben Sghaier M, Ghedira K, Dijoux Franca MG, Chekir-Ghedira L. Ethyl
568 acetate extract and its major constituent, isorhamnetin 3-O-rutinoside, from Nitraria retusa leaves,
569 promote apoptosis of human myelogenous erythroleukaemia cells. Cell Prolif. 2011;44(5):453-61. doi:
570 10.1111/j.1365-2184.2011.00772.x. PubMed PMID: 21951288.
571 35. Leroy B, Girard L, Hollestelle A, Minna JD, Gazdar AF, Soussi T. Analysis of TP53 mutation
572 status in human cancer cell lines: a reassessment. Hum Mutat. 2014;35(6):756-65. doi:
573 10.1002/humu.22556. PubMed PMID: 24700732; PubMed Central PMCID: PMCPMC4451114.
574 36. Chen B, Co C, Ho CC. Cell shape dependent regulation of nuclear morphology. Biomaterials.
575 2015;67:129-36. doi: 10.1016/j.biomaterials.2015.07.017. PubMed PMID: 26210179; PubMed Central
576 PMCID: PMCPMC4626019.
577 37. Hiromura K, Pippin JW, Fero ML, Roberts JM, Shankland SJ. Modulation of apoptosis by
578 the cyclin-dependent kinase inhibitor p27(Kip1). J Clin Invest. 1999;103(5):597-604. doi:

bioRxiv preprint doi: https://doi.org/10.1101/441162; this version posted October 11, 2018. The copyright holder for this preprint (which was not certified by peer review) is the author/funder, who has granted bioRxiv a license to display the preprint in perpetuity. It is made available under a CC-BY 4.0 International license.

10.1172/JCI5461. PubMed PMID: 10074476; PubMed Central PMCID: PMCPMC408127.

38. Sutherland RL, Watts CK, Musgrove EA. Cyclin gene expression and growth control in normal and neoplastic human breast epithelium. J Steroid Biochem Mol Biol. 1993;47(1-6):99-106. PubMed PMID: 8274447.

39. Murad H, Hawat M, Ekhtiar A, AlJapawe A, Abbas A, Darwish H, et al. Induction of G1-phase cell cycle arrest and apoptosis pathway in MDA-MB-231 human breast cancer cells by sulfated polysaccharide extracted from Laurencia papillosa. Cancer Cell Int. 2016;16:39. doi: 10.1186/s12935-016-0315-4. PubMed PMID: 27231438; PubMed Central PMCID: PMCPMC4881178.

40. Aleem E, Kiyokawa H, Kaldis P. Cdc2-cyclin E complexes regulate the G1/S phase transition. Nat Cell Biol. 2005;7(8):831-6. doi: 10.1038/ncb1284. PubMed PMID: 16007079.

Supporting Information

S1 Figure. Cell viability treated with Isohamnetin-3-O-rutinoside in the A549 and NCI-H1299 cells. The viabilities of A549 and NCI-H1299 cells. A549 and NCI-H1299 cells were treated for 48 h with Isohamnetin-3-O-rutinoside. Viability was analyzed by MTS assay. The experiments were performed at least three times..

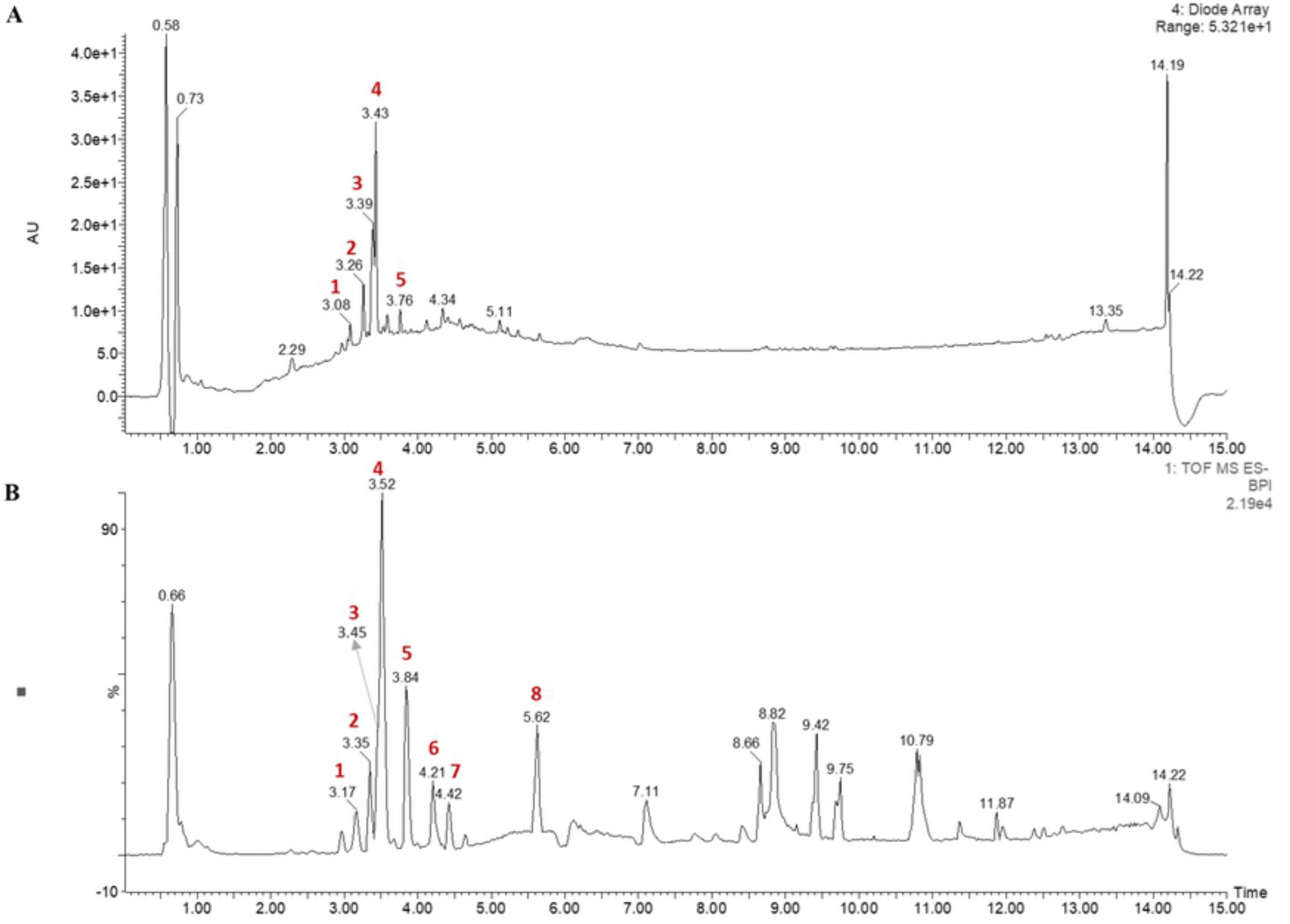
A
4: Diode Array
Range: 5.321e+1
AU
0.58
0.73
4
3.43
3
3.39
2
3.26
1
3.08
5
3.76
2.29
4.34
5.11
13.35
14.19
14.22
B
1: TOF MS ES-
BPI
2.19e4
%
0.66
4
3.52
3
3.45
5
3.84
2
3.35
1
3.17
6
4.21
7
4.42
8
5.62
7.11
8.66
8.82
9.42
9.75
10.79
11.87
14.09
14.22
Time

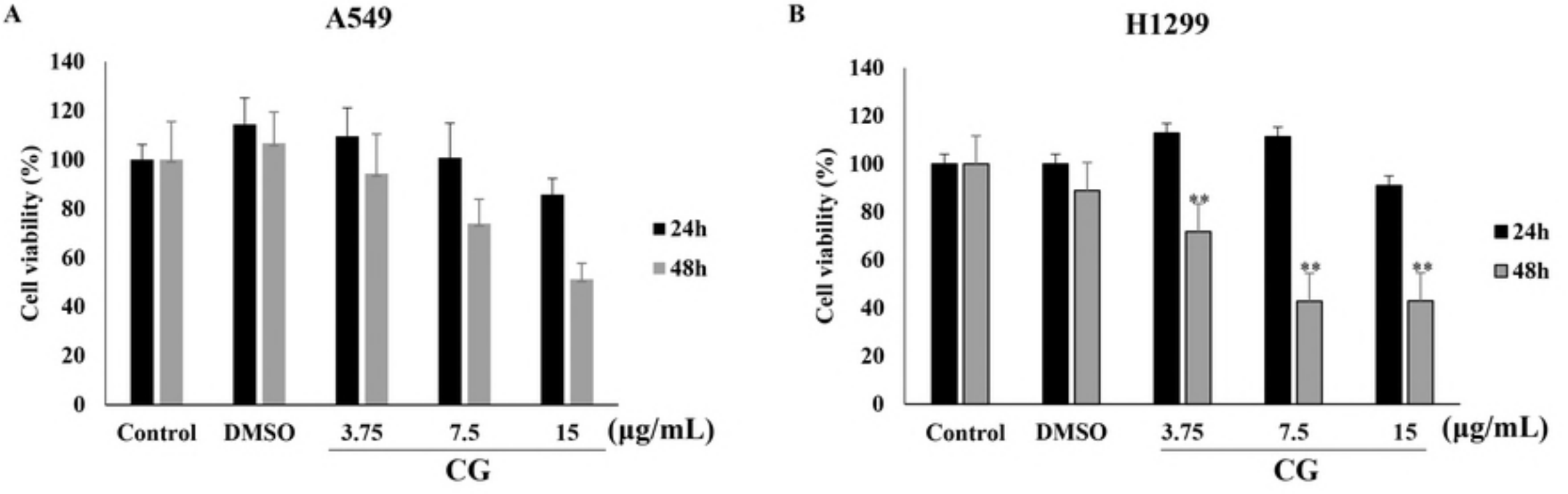
A
A549
Cell viability (%)
140
120
100
80
60
40
20
0
24h
48h
Control
DMSO
3.75
7.5
15
(μg/mL)
CG
B
H1299
Cell viability (%)
140
120
100
80
60
40
20
0
**
**
**
24h
48h
Control
DMSO
3.75
7.5
15
(μg/mL)
CG

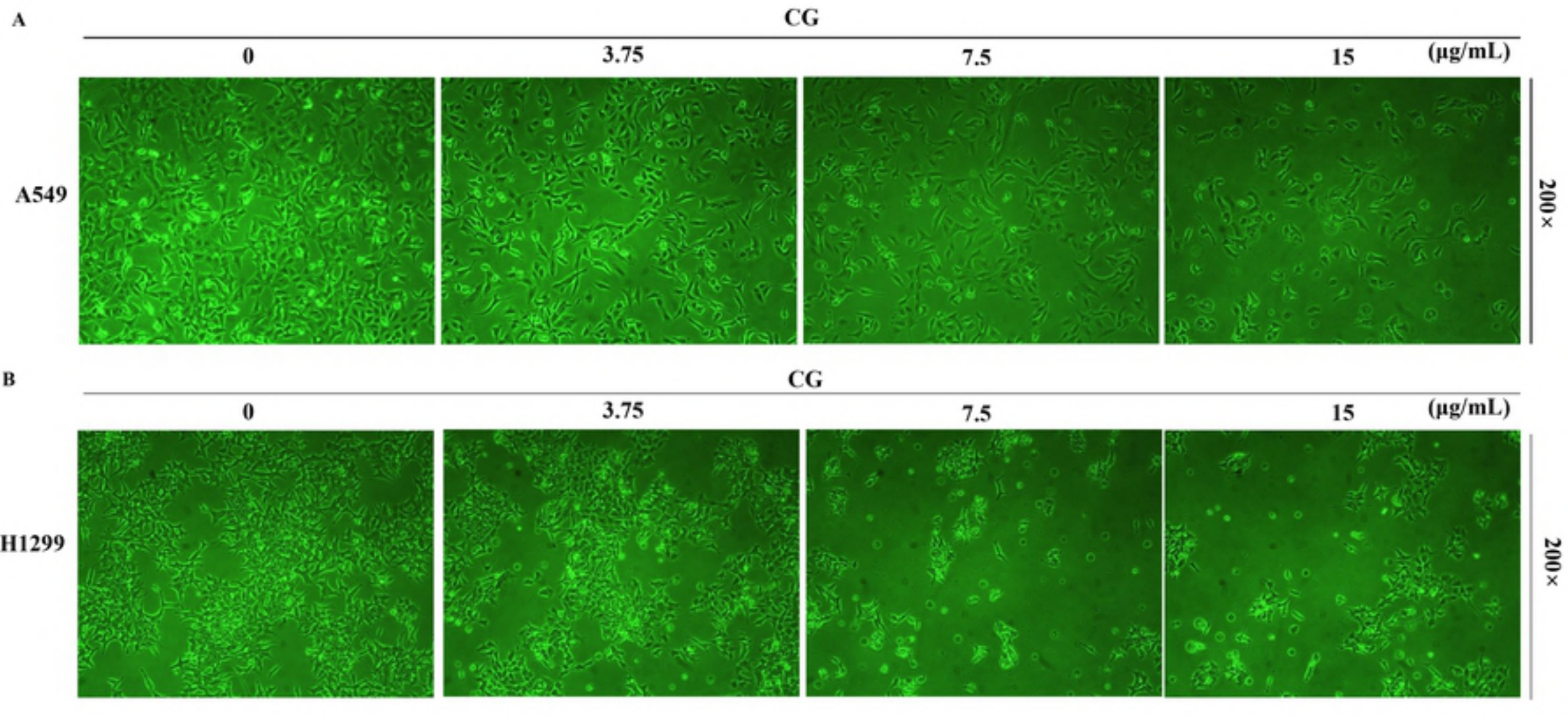
A
CG
0
3.75
7.5
15
(μg/mL)
A549
200×
B
CG
0
3.75
7.5
15
(μg/mL)
H1299
200×

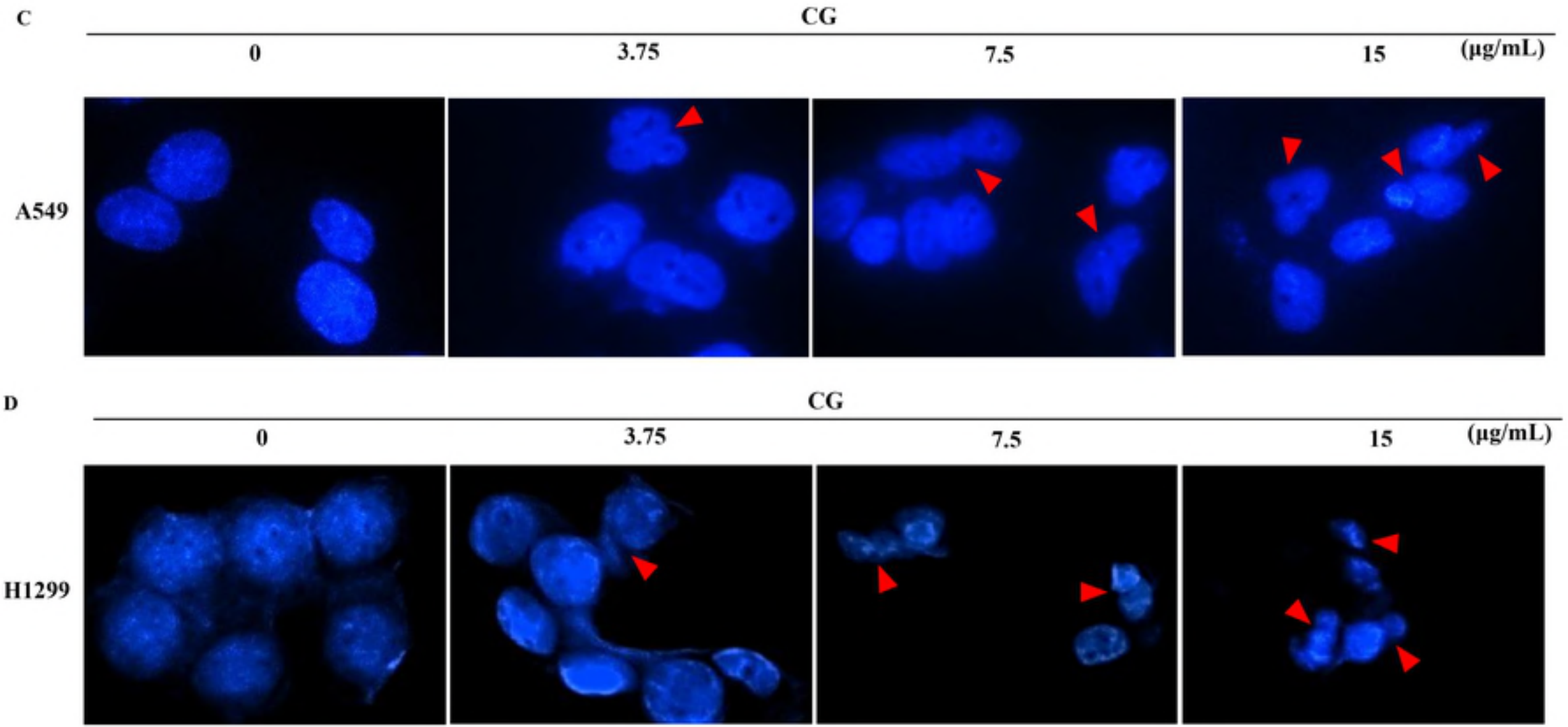
C
CG
0
3.75
7.5
15
(μg/mL)
A549
D
CG
0
3.75
7.5
15
(μg/mL)
H1299

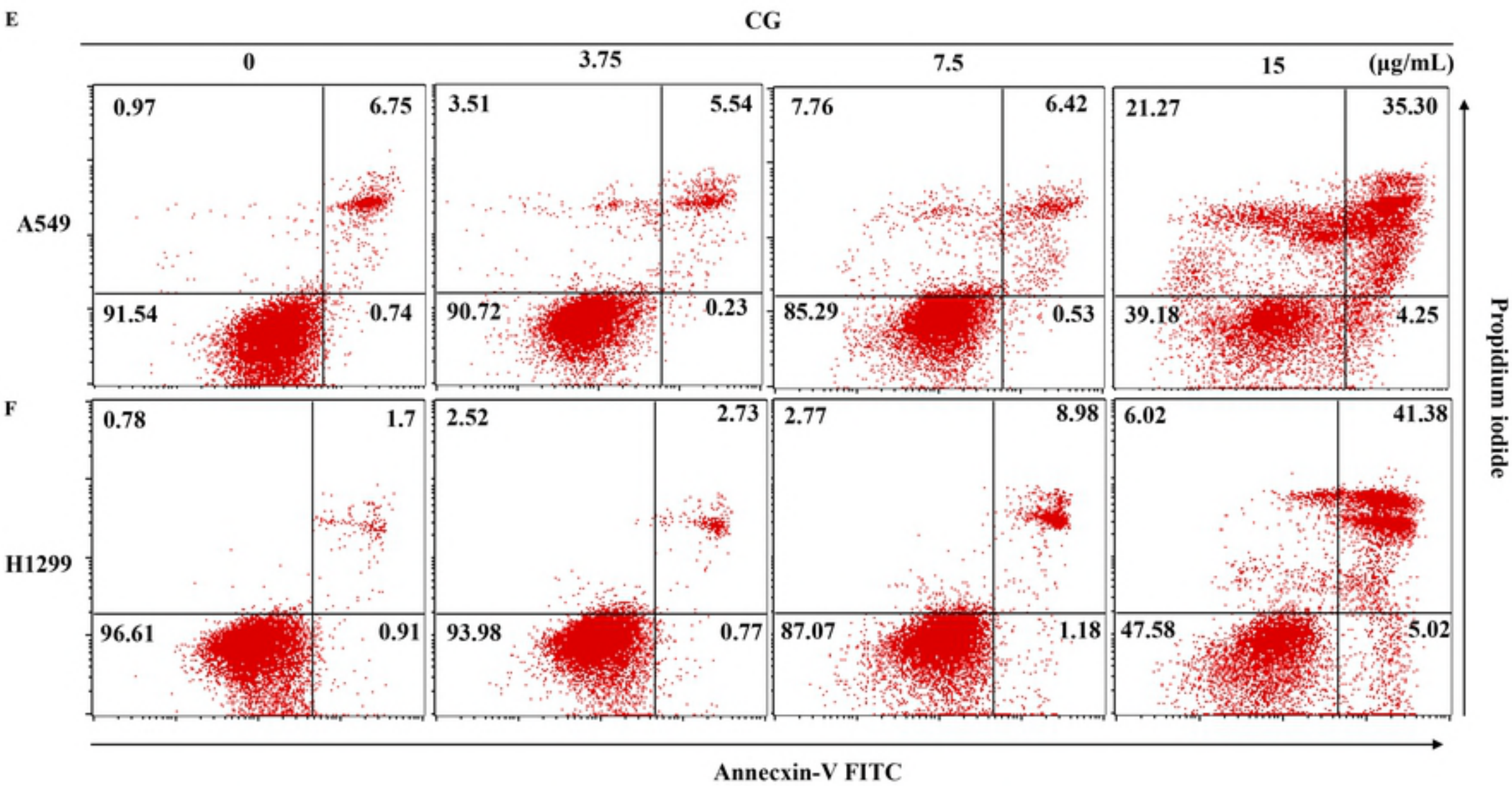
E
CG
0
3.75
7.5
15
(μg/mL)
A549
0.97
6.75
91.54
0.74
3.51
5.54
90.72
0.23
7.76
6.42
85.29
0.53
21.27
35.30
39.18
4.25
F
H1299
0.78
1.7
96.61
0.91
2.52
2.73
93.98
0.77
2.77
8.98
87.07
1.18
6.02
41.38
47.58
5.02
Propidium iodide
Annecxin-V FITC

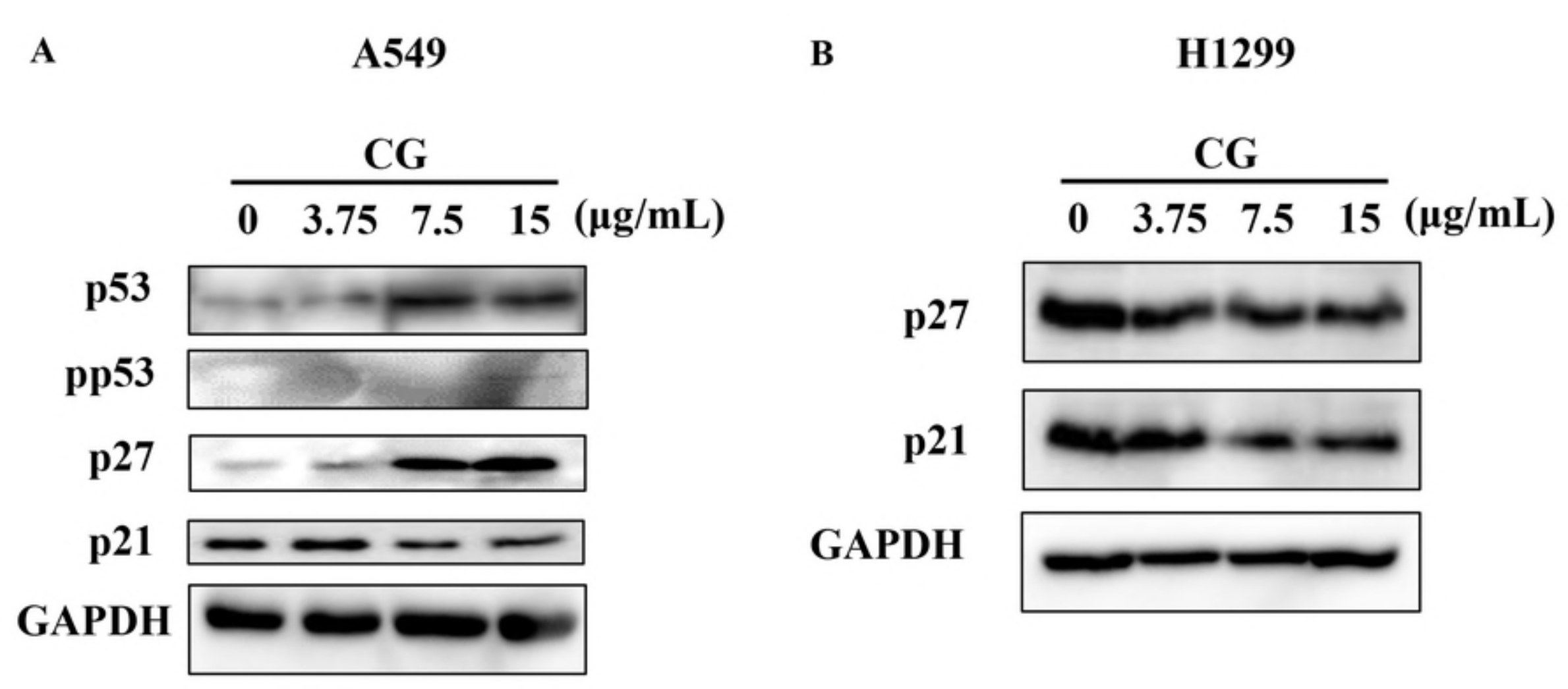
A
A549
CG
0 3.75 7.5 15 (μg/mL)
p53
pp53
p27
p21
GAPDH
B
H1299
CG
0 3.75 7.5 15 (μg/mL)
p27
p21
GAPDH

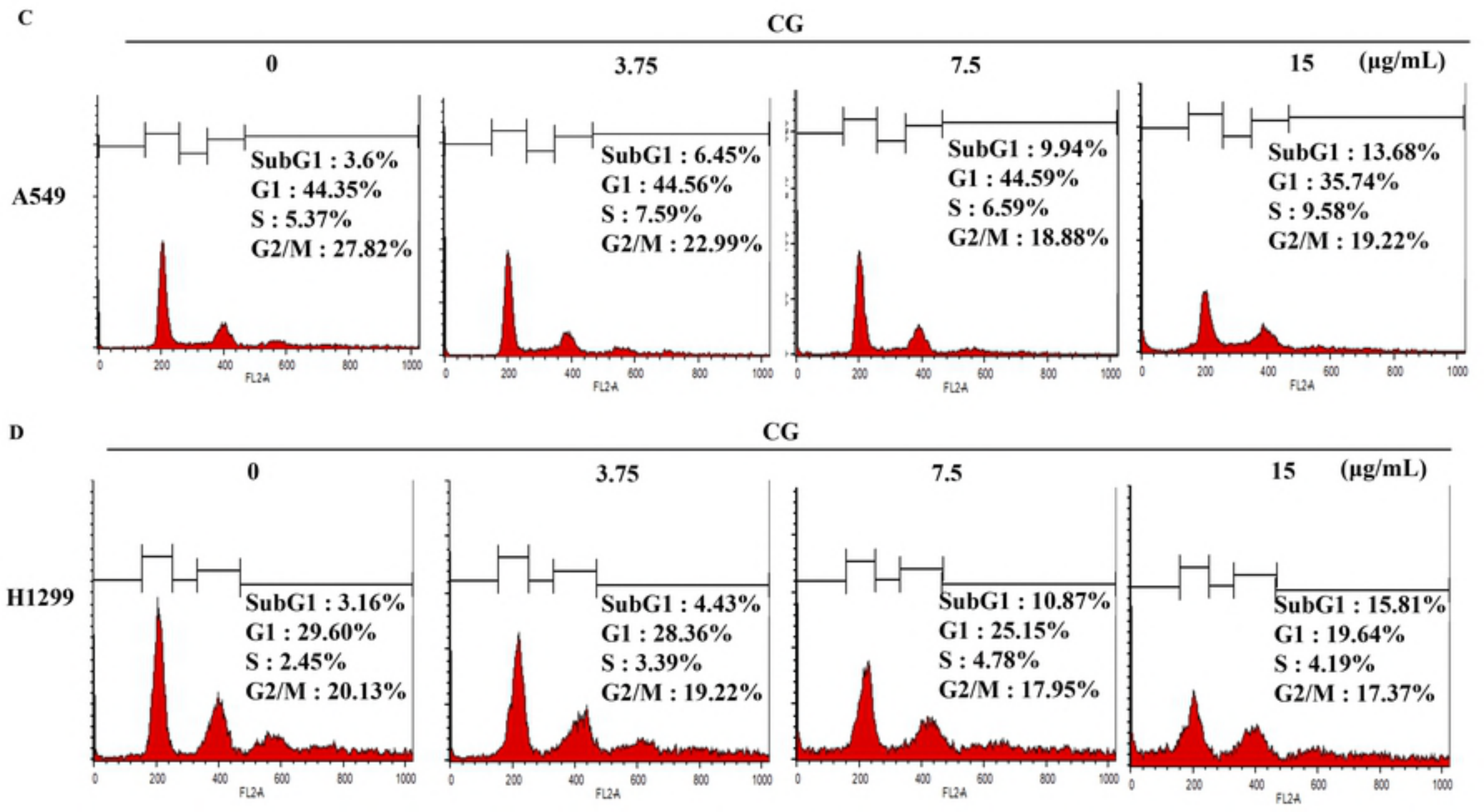
C
CG
0
3.75
7.5
15
(μg/mL)
A549
SubG1 : 3.6%
G1 : 44.35%
S : 5.37%
G2/M : 27.82%
SubG1 : 6.45%
G1 : 44.56%
S : 7.59%
G2/M : 22.99%
SubG1 : 9.94%
G1 : 44.59%
S : 6.59%
G2/M : 18.88%
SubG1 : 13.68%
G1 : 35.74%
S : 9.58%
G2/M : 19.22%
FL2-A
D
CG
0
3.75
7.5
15
(μg/mL)
H1299
SubG1 : 3.16%
G1 : 29.60%
S : 2.45%
G2/M : 20.13%
SubG1 : 4.43%
G1 : 28.36%
S : 3.39%
G2/M : 19.22%
SubG1 : 10.87%
G1 : 25.15%
S : 4.78%
G2/M : 17.95%
SubG1 : 15.81%
G1 : 19.64%
S : 4.19%
G2/M : 17.37%
FL2-A

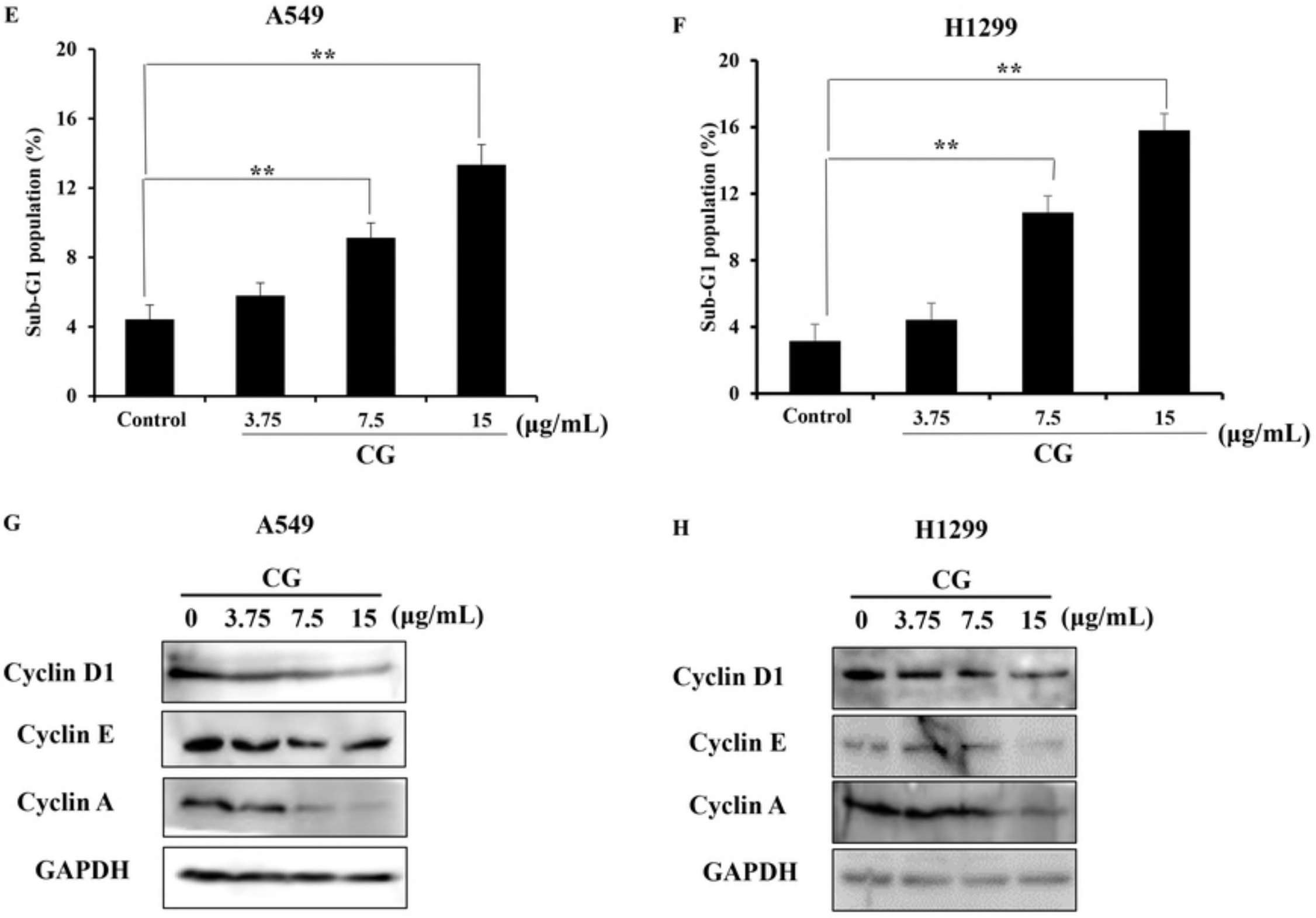
E
A549
Sub-G1 population (%)
20
16
12
8
4
0
**
**
Control
3.75
7.5
15
(μg/mL)
CG
F
H1299
Sub-G1 population (%)
20
16
12
8
4
0
**
**
Control
3.75
7.5
15
(μg/mL)
CG
G
A549
CG
0 3.75 7.5 15 (μg/mL)
Cyclin D1
Cyclin E
Cyclin A
GAPDH
H
H1299
CG
0 3.75 7.5 15 (μg/mL)
Cyclin D1
Cyclin E
Cyclin A
GAPDH

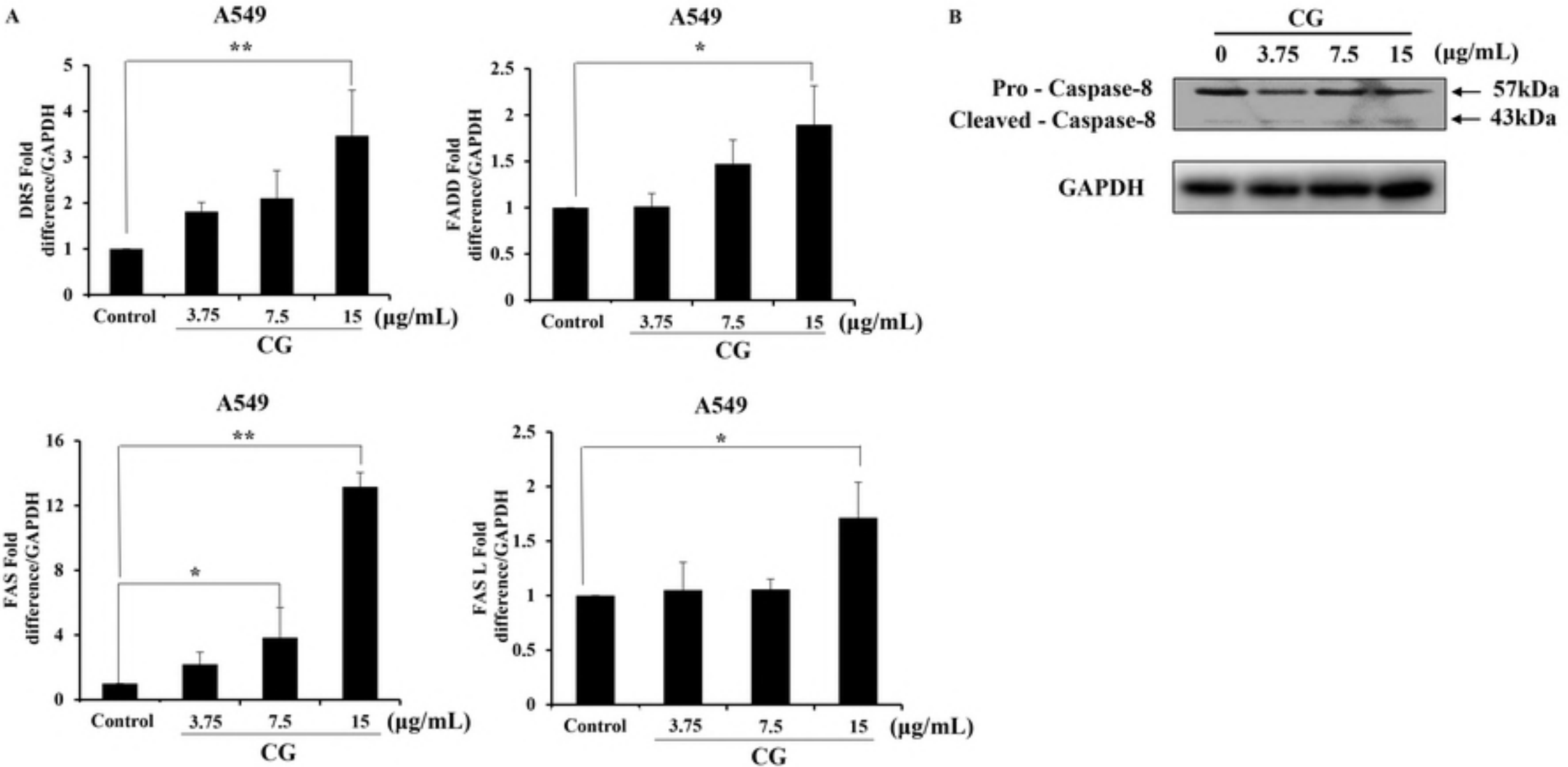
A
A549
**
DR5 Fold difference/GAPDH
Control
3.75
7.5
15
(μg/mL)
CG
A549
*
FADD Fold difference/GAPDH
Control
3.75
7.5
15
(μg/mL)
CG
B
CG
0
3.75
7.5
15
(μg/mL)
Pro - Caspase-8
Cleaved - Caspase-8
57kDa
43kDa
GAPDH
A549
**
*
FAS Fold difference/GAPDH
Control
3.75
7.5
15
(μg/mL)
CG
A549
*
FAS L Fold difference/GAPDH
Control
3.75
7.5
15
(μg/mL)
CG

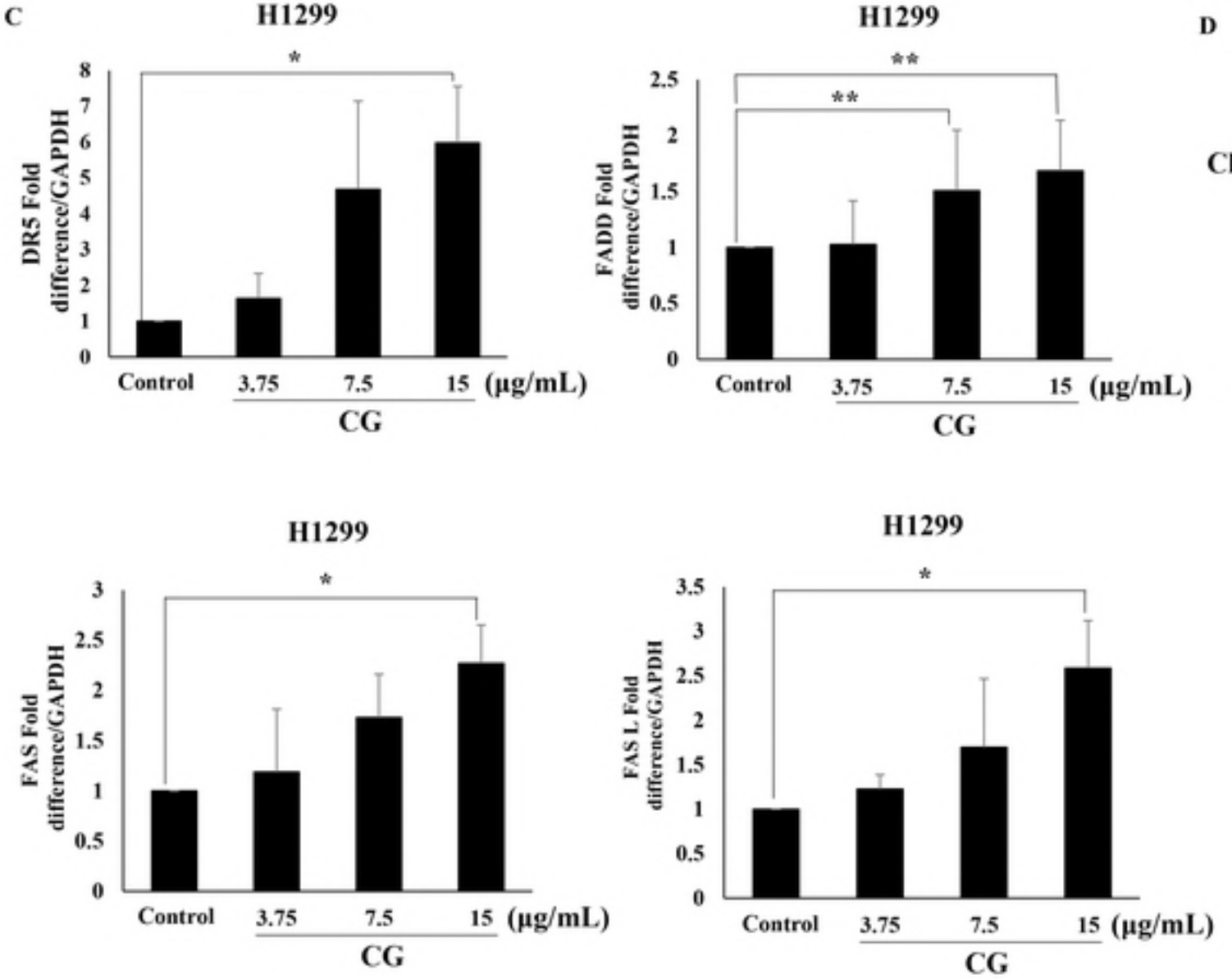
C
H1299
DR5 Fold difference/GAPDH
*
Control
3.75
7.5
15
(μg/mL)
CG
H1299
FADD Fold difference/GAPDH
**
**
Control
3.75
7.5
15
(μg/mL)
CG
H1299
FAS Fold difference/GAPDH
*
Control
3.75
7.5
15
(μg/mL)
CG
H1299
FAS L Fold difference/GAPDH
*
Control
3.75
7.5
15
(μg/mL)
CG
D
CG
0
3.75
7.5
15
(μg/mL)
Pro - Caspase-8
Cleaved - Caspase-8
57kDa
43kDa
GAPDH

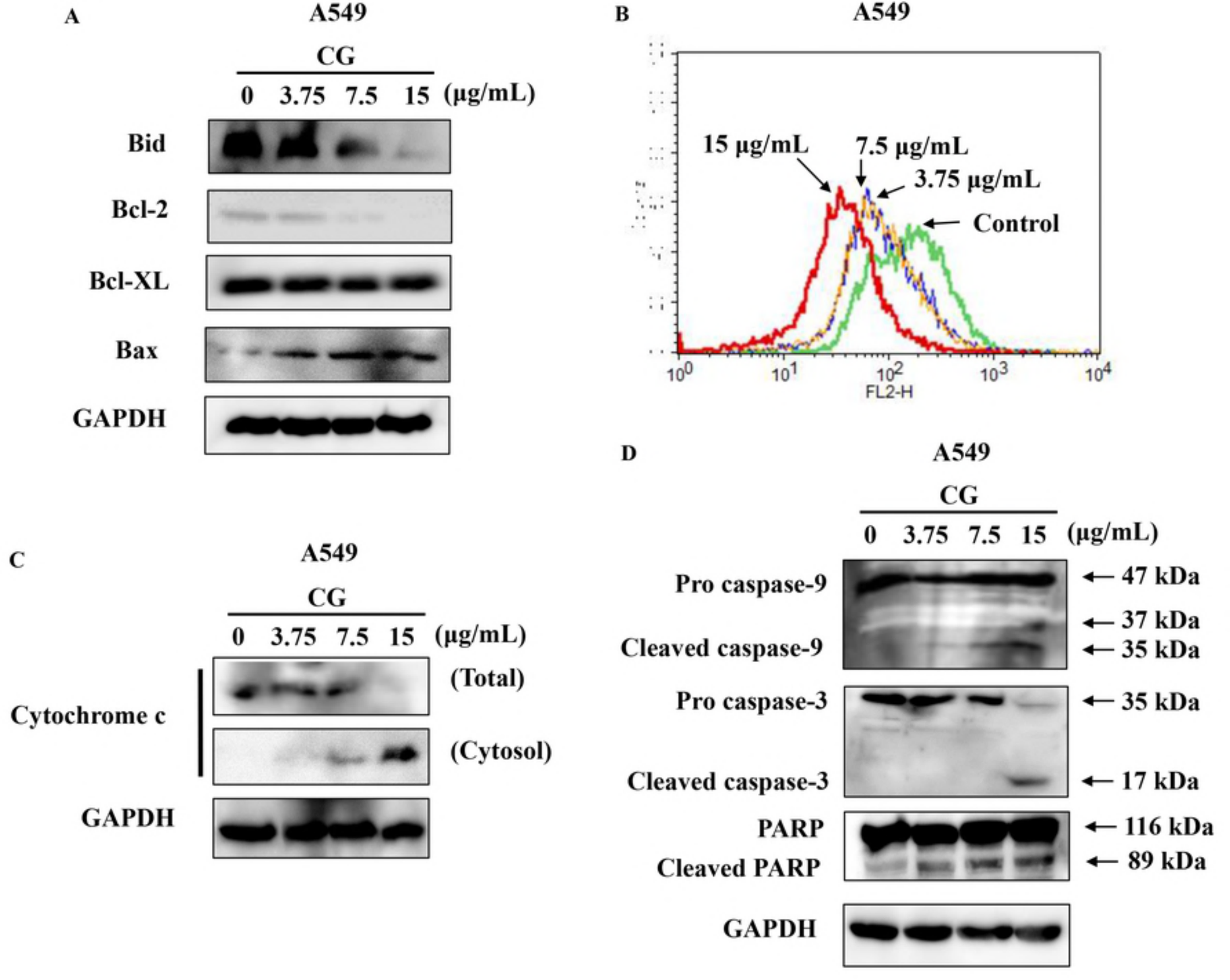
A
A549
CG
0 3.75 7.5 15 (μg/mL)
Bid
Bcl-2
Bcl-XL
Bax
GAPDH
B
A549
15 μg/mL
7.5 μg/mL
3.75 μg/mL
Control
10^0 10^1 10^2 10^3 10^4
FL2-H
C
A549
CG
0 3.75 7.5 15 (μg/mL)
Cytochrome c
(Total)
(Cytosol)
GAPDH
D
A549
CG
0 3.75 7.5 15 (μg/mL)
Pro caspase-9
Cleaved caspase-9
47 kDa
37 kDa
35 kDa
Pro caspase-3
Cleaved caspase-3
35 kDa
17 kDa
PARP
Cleaved PARP
116 kDa
89 kDa
GAPDH

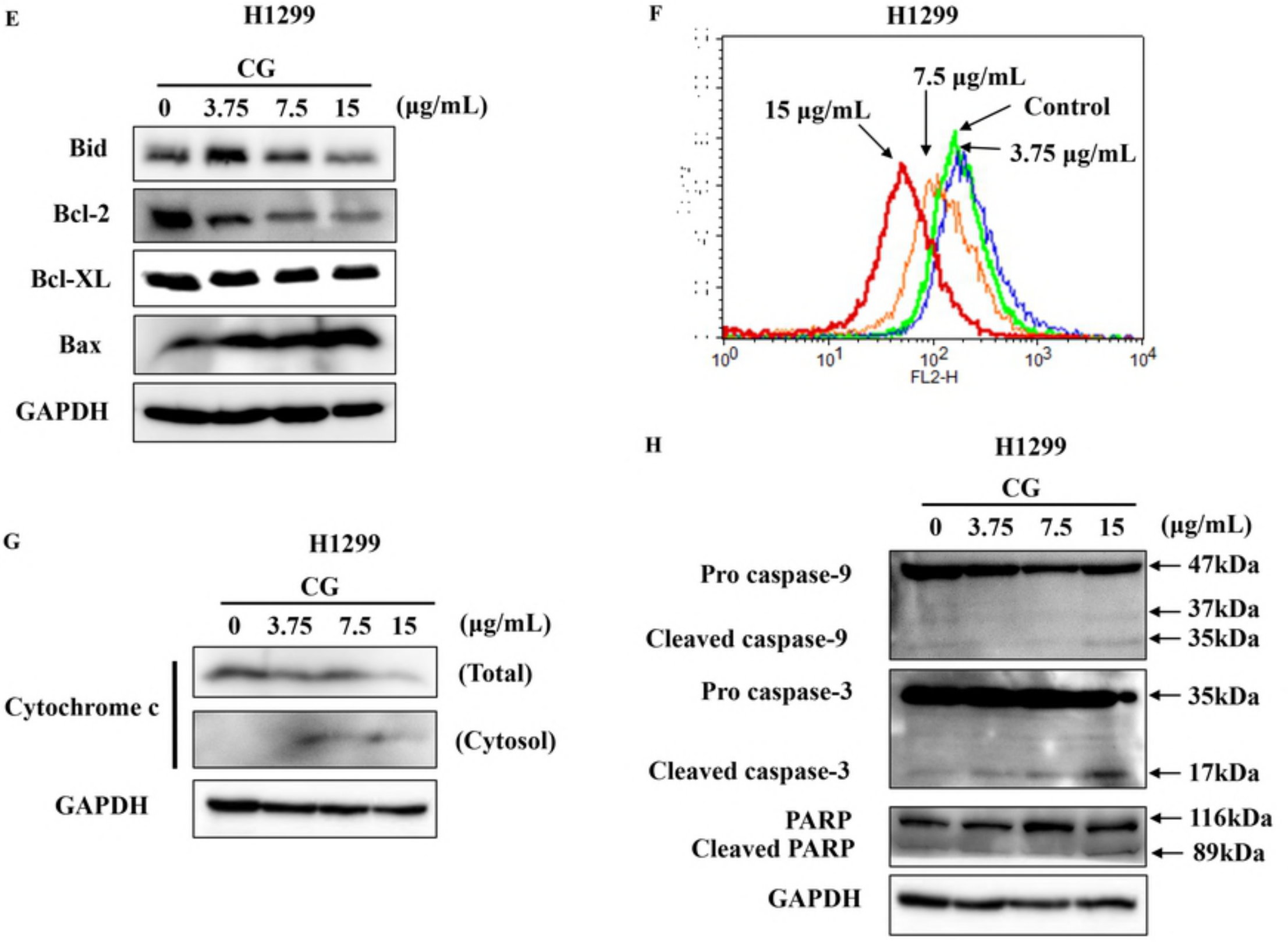
E
H1299
CG
0 3.75 7.5 15 (μg/mL)
Bid
Bcl-2
Bcl-XL
Bax
GAPDH
F
H1299
7.5 μg/mL
15 μg/mL
Control
3.75 μg/mL
10^0 10^1 10^2 10^3 10^4
FL2-H
G
H1299
CG
0 3.75 7.5 15 (μg/mL)
Cytochrome c
(Total)
(Cytosol)
GAPDH
H
H1299
CG
0 3.75 7.5 15 (μg/mL)
Pro caspase-9
Cleaved caspase-9
47kDa
37kDa
35kDa
Pro caspase-3
Cleaved caspase-3
35kDa
17kDa
PARP
Cleaved PARP
116kDa
89kDa
GAPDH

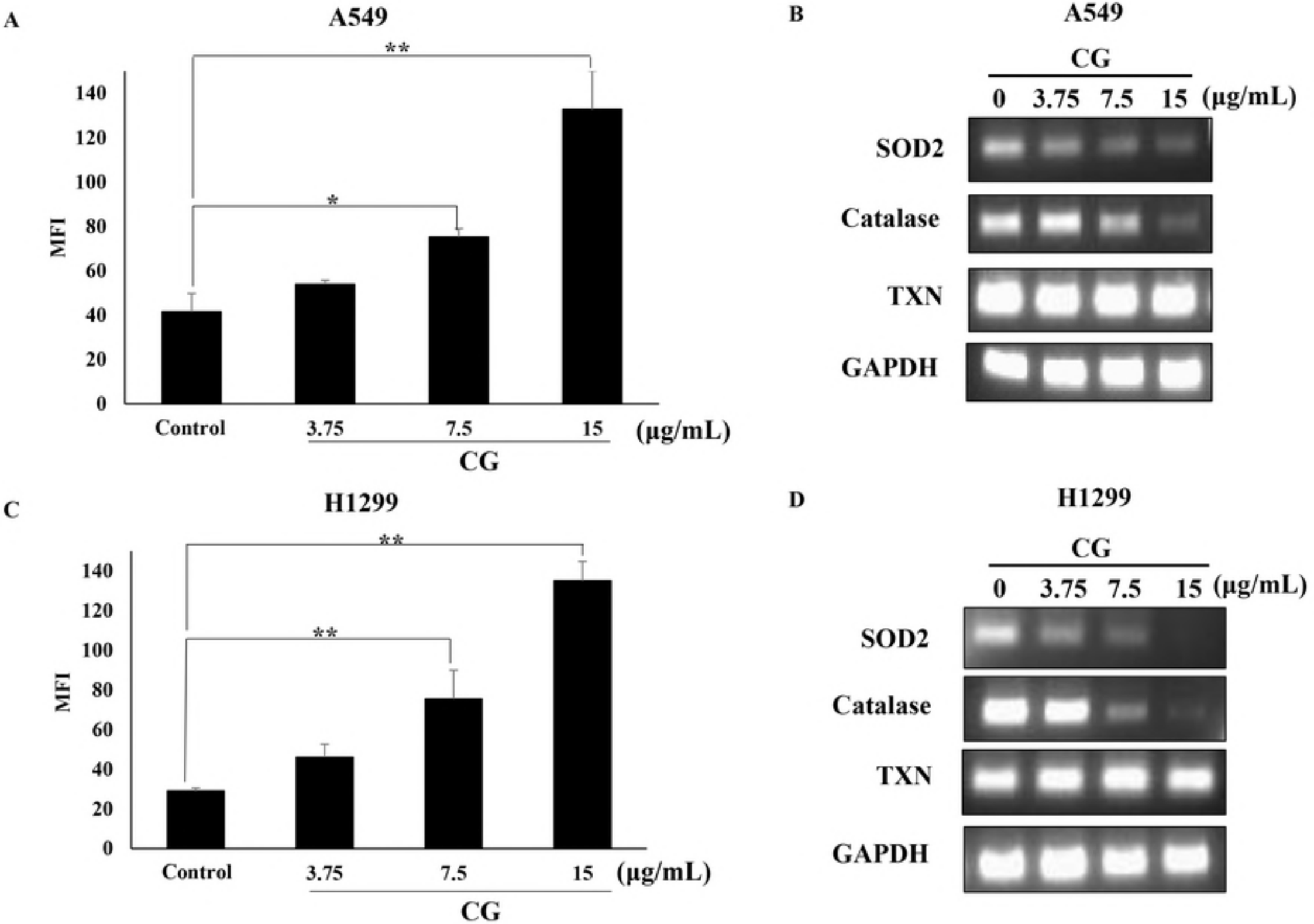
A
A549
**
*
140
120
100
80
60
40
20
0
MFI
Control
3.75
7.5
15
(μg/mL)
CG
B
A549
CG
0
3.75
7.5
15
(μg/mL)
SOD2
Catalase
TXN
GAPDH
C
H1299
**
**
140
120
100
80
60
40
20
0
MFI
Control
3.75
7.5
15
(μg/mL)
CG
D
H1299
CG
0
3.75
7.5
15
(μg/mL)
SOD2
Catalase
TXN
GAPDH

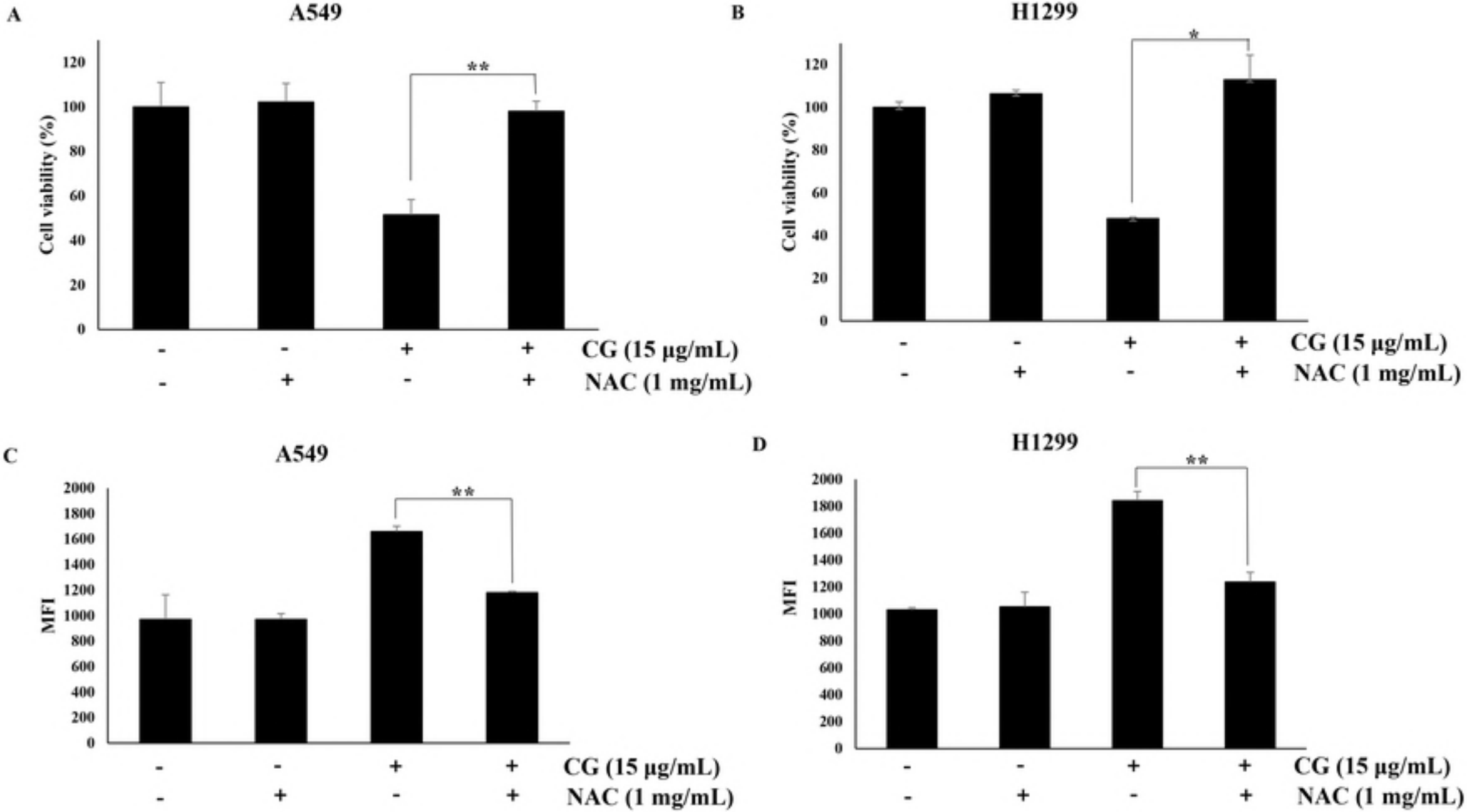
A
A549
Cell viability (%)
120
100
80
60
40
20
0
**
- - + + CG (15 μg/mL)
- + - + NAC (1 mg/mL)
B
H1299
Cell viability (%)
120
100
80
60
40
20
0
*
- - + + CG (15 μg/mL)
- + - + NAC (1 mg/mL)
C
A549
MFI
2000
1800
1600
1400
1200
1000
800
600
400
200
0
**
- - + + CG (15 μg/mL)
- + - + NAC (1 mg/mL)
D
H1299
MFI
2000
1800
1600
1400
1200
1000
800
600
400
200
0
**
- - + + CG (15 μg/mL)
- + - + NAC (1 mg/mL)

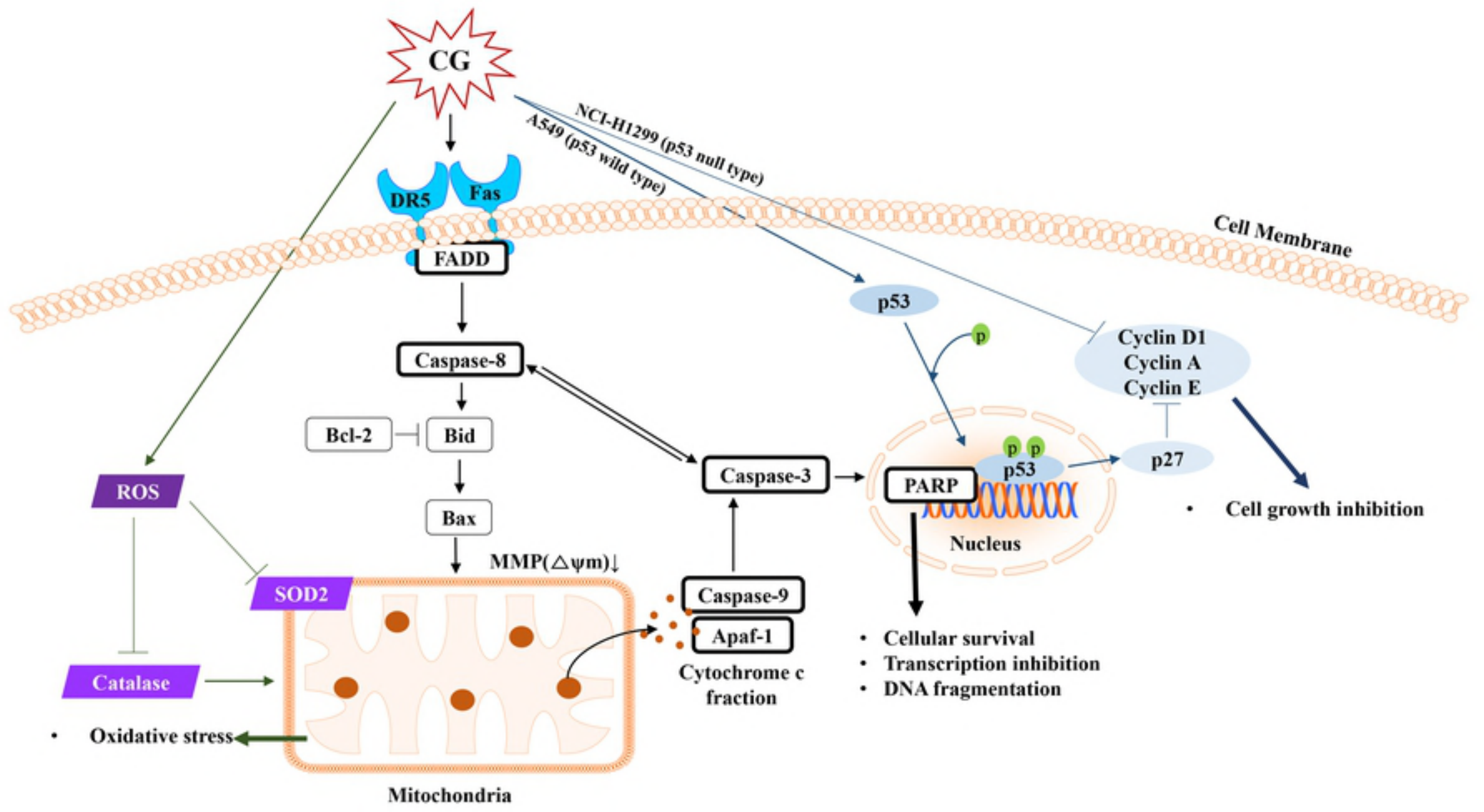
CG
NCI-H1299 (p53 null type)
A549 (p53 wild type)
DR5
Fas
FADD
Cell Membrane
p53
Caspase-8
Bcl-2
Bid
Bax
ROS
SOD2
Catalase
Oxidative stress
MMP(△ψm)↓
Mitochondria
Caspase-9
Apaf-1
Cytochrome c fraction
Caspase-3
PARP
p53
Nucleus
Cyclin D1
Cyclin A
Cyclin E
p27
Cell growth inhibition
Cellular survival
Transcription inhibition
DNA fragmentation